THE UNIVERSITY OF OKLAHOMA

GRADUATE COLLEGE

THE MAGNETIZATION OF $FeBO_3$ IN THE CRITICAL REGION

A DISSERTATION

SUBMITTED TO THE GRADUATE FACULTY

in partial fulfillment of the requirements for the

degree of

DOCTOR OF PHILOSOPHY

BY

DAVID MACK WILSON

Norman, Oklahoma

1975

THE MAGNETIZATION OF $FeBO_3$ IN THE CRITICAL REGION

APPROVED BY

Leonard Broerman

Jesse Levy

Stanley E. Babb, Jr.

J. Neal Shulman

DISSERTATION COMMITTEE

ACKNOWLEDGEMENTS

Sincere appreciation is extended to Professor Sybrand Broersma for his guidance throughout the experiment and his invaluable criticisms during the preparation of this manuscript.

The author gives special thanks to Larry Walls for his assistance and advice during the entire investigation.

Finally, to my wife, Theresa, I express my gratitude for her constant encouragement and cheerfulness.

TABLE OF CONTENTS

TABLE OF CONTENTS (Cont'd.)

LIST OF TABLES

LIST OF FIGURES

LIST OF FIGURES (Cont'd.)

CHAPTER I

INTRODUCTION

This dissertation is an investigation of the magnetization of iron borate $FeBO_3$ near the Curie temperature as a function of pressure, temperature, and magnetic field. Iron borate is a green, transparent, canted antiferromagnet with a Curie temperature of 348 K.[1,2] Early investigators were interested in iron borate because the ratio of Faraday rotation to optical absorption is large. However, birefringence limits the magneto-optical potential of single crystals.[3,4] The spontaneous sublattice magnetizations of $FeBO_3$ follow a J=5/2 Brillouin curve from 4 to 293 K.[5,6,7] In the vicinity of the Curie temperature mean field theory no longer agrees with experiment and is replaced by scaling theory. Scaling theory uses critical exponents to describe the change in magnetization with temperature and magnetic field. The aim of this investigation is to find these critical exponents for iron borate and to determine the effect of pressure on the magnetization. Values for two of the critical exponents have been reported.[8,9] These exponents relate the spontaneous magnetization to the temperature and the magnetization at T_c to the magnetic field. Besides making an independent measurement of these exponents, two additional ones are determined. The additional exponents relate the initial differential susceptibility

below T_c and initial susceptibility above T_c to the temperature. The third independent parameter, pressure, causes a linear shift in the Curie temperature.

The design of the experiment is controlled by the choice of the sample and the measurements desired. The sample holder must be strong enough to withstand the pressure at elevated temperatures and also be relatively non-magnetic. This requirement is met by a beryllium-copper alloy. With the sample inside a pressure vessel it is impractical to measure its magnetization by vibrating the sample. Thus, a modification of the vibrating coil technique described by D. O. Smith, K. Dwight, and N. Menyuk[10,11] is used. This modification vibrates the coils perpendicular to the magnetizing field rather than parallel to it. The principle behind a vibrating sample or vibrating coil magnetometer is Faraday's law. Relative motion between the magnetic induction field of the sample and the coil induces a voltage in the coil proportional to the sample magnetization. The magnetization is then obtained by calibration with a known induction field. The vibrating sample technique is easier to use because non-uniformity in the applied magnetic field does not induce a voltage in the coil. With the vibrating coil technique one has more ability to control the environment around the sample.

The Curie temperature of iron borate is 75°C. Near this temperature the environment can be controlled relatively easily. A circulating fluid from a heat bath sets the temperature. A simple jack pump using hydraulic fluid controls the pressure from 0 to 3 kilobar. The applied magnetic field is limited to

5 kilo-oersted for the size gap needed between the pole pieces to contain the vibrating coil and sample. The magnetic quantities are given in electromagnetic units because of their convenient size and general usage in this field.

The iron borate was made by reacting Fe_2O_3 with B_2O_3 in a furnace. The initial reaction followed a general method published by J. C. Joubert, T. Shirk, W. B. White, and Rustum Roy.[12] Conditions were modified until an acceptable green magnetic sample was obtained. The modified procedure gives a powder consisting of platelets 1 to 5 microns in diameter. A sample made by this procedure was checked by chemical analysis and X-ray diffraction to determine its purity.

The relative magnetization of iron borate is measured at selected values of temperature, magnetic field, and pressure. A 10 gram sample is used because $FeBO_3$ has a relatively low magnetization. Because the beryllium-copper sample holder contains a small amount of cobalt, the signal from the sample holder is significant. The demagnetizing field correction is small because of the low magnetization of $FeBO_3$. When pressure is applied, the overall sample dimensions are changed and a correction for this effect is necessary.

I. E. Dzialoshinskii[13] published a thermodynamic theory for canted antiferromagnets in 1957. His theory minimizes a power series expansion for the magnetic part of the free energy near T_c. He uses the theory to explain the magnetic behavior of α-Fe_2O_3. A. S. Borovik-Romanov and V. I. Ozhogin[14] applied the theory to single crystals of $CoCO_3$ in 1960.

Dzialoshinskii's theory also can explain the magnetic properties of iron borate. For this dissertation three modifications or extensions are necessary, however. First, the temperature dependence of the coefficients in the free energy are chosen to make the theory agree more closely near T_c with the current scaling theory. Second, the single crystal results are extended to apply to a powdered sample, possibly an aligned one. This extension is easy due to the following characteristic of $FeBO_3$. The anisotropy field is very low in the basal plane of the crystal which contains the spontaneous magnetization. In an applied magnetic field the magnetization remains essentially in the basal plane but rotates so that it has a maximum component along the field. This reduces the averaging of the magnetization in a powdered sample to a mathematically simple pseudo two-dimensional problem. Third, a theory for the effect of pressure on a canted antiferromagnet is developed within the above thermodynamic framework.

The data is analyzed using the modified theory. The Curie temperature, four critical exponents from scaling theory, and the change of T_c with pressure are determined. The Curie temperature and two critical exponents are compared to published values.

CHAPTER II

EQUIPMENT

The magnetization of a material is a function of temperature, applied magnetic field, and hydrostatic pressure. The design and calibration of the equipment used to measure magnetization, magnetic field, temperature, and pressure will be described in turn.

Magnetization

The effect of a small sample in a magnetic field can be represented by a dipole field. The strength of this dipole field can be determined from the induced voltage created by a relative motion between a pick-up coil and a sample by applying Faraday's induction law. With a vibrating sample magnetometer only the field of the sample induces a voltage in the pick-up coils. However, control of the environment around such a moving sample is restricted. On the other hand with a vibrating coil magnetometer, the curvature of the applied magnetic field also induces a voltage in the vibrating pick-up coil. Now, however, the sample is stationary and its environment is more easily controlled.

There are two basic configurations of vibrating coils which can be used to sense a dipole field. D. O. Smith[10] in 1956 reported on the first configuration in which the coil vibrates parallel to the axis of symmetry of the dipole field. At the same time he also described how to design an optimum pick-up coil

once the dipole to coil spacing is set. A magnetometer based on the second configuration in which the pick-up coil vibrates perpendicularly to the dipole's axis is used in this work. To reduce the sensitivity to the location of the sample, two coils, one on each side of the sample, are employed. A coordinate system for the magnetometer is defined in Figure 1.

The dipole moment of the sample $\vec{m}_1$ and applied magnetic field are directed along the z axis. The y axis is vertical and the x axis is perpendicular to the magnetic field and chosen to complete a Cartesian coordinate system. The origin of the system is at the center of the sample. The displacement of the center of the vibrating pick-up coils with time t is

$$x = x_o + A_1 \sin\omega_1 t$$

where

x_o = distance from the sample to the axis of coils at t = 0,

ω_1 = frequency of vibration, and

A_1 = amplitude of vibration.

The induced voltage V_1 in the N turns of each pick-up coil at position x is

$$V_1(x,t) = [-\partial/\partial x \ (\sum_1^N \int B_z da_i)] \ dx/dt$$

$$= A_1\omega_1 \cos\omega_1 t \ [-\partial/\partial x \ (\sum_1^N \int B_z da_i)]$$

where

B_z = z component of the magnetic induction created by $\vec{m}_1$,

da_i = differential area element in loop i, and

N = number of loops in a coil.

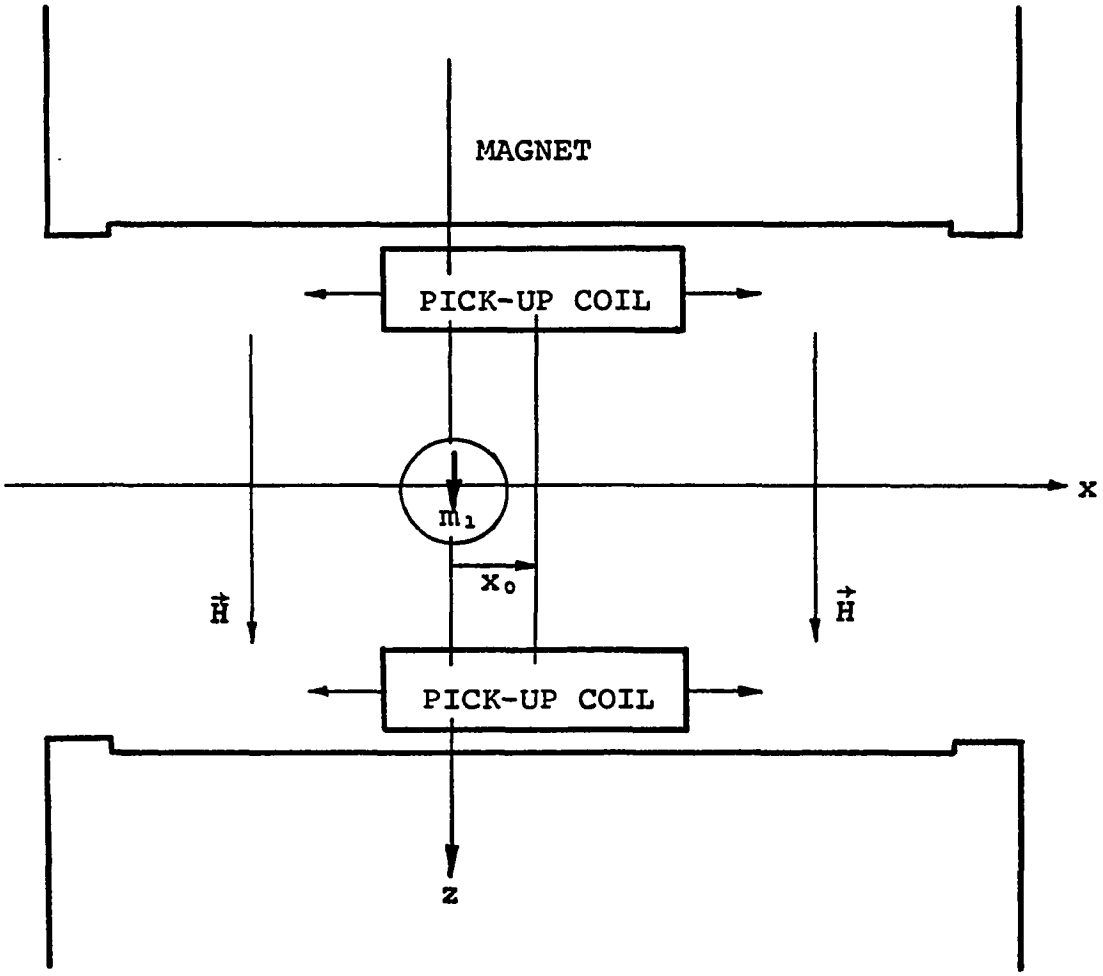

Figure 1. Coordinate System for the Sample and Pick-up Coils in the Magnetometer. The y axis is vertical. Flux from the magnetic dipole moment of the sample $\vec{m}_1$ causes an induced voltage in the pick-up coils as they are vibrated parallel to the x axis.

The rms voltage from the induced AC voltage V_1 will be proportional to the magnetic moment of the sample. The proportionality coefficient can be a function of the shape of the sample. However, for small samples only the dipole field is important. Therefore, the proportionality coefficient is a unique constant which is easily obtained by calibration.

To study the operation of the magnetometer in detail we switched the roles of the fixed sample and vibrating pick-up coils. The sample was replaced by a sample coil which used AC current and the pick-up coils were held stationary. The dipole field $(B_z)_{AC}$ of the sample coil is

$$(B_z)_{AC} = (B_z)_{DC} \sin\omega_2 t$$

where

$(B_z)_{DC}$ = dipole field resulting when DC current equivalent to the peak AC and

ω_2 = frequency of the AC current (60 Hz).

The rms voltage $(V_2)_{rms}$ induced in each pick-up coil, (now stationary), is

$$[V_2(x)]_{rms} = (\omega_2/\sqrt{2}) \sum_1^N \int (B_z)_{DC} \, da_i$$

The measured relative voltage $(V_2)_{rms}$ as a function of x is shown in Figure 2. The flux $\Phi_2(x)$ given by

$$\Phi_2(x) = \sum_1^N \int (B_z)_{DC} \, da_i$$

is calculated with the aid of a computer as described in Appendix I.

The values of $(V_2)_{rms}$ and Φ_2, scaled to agree at x equal to zero, are compared in Figure 2. The calculated and measured values basically agree. The small differences can be due to the small quadrupole field of the coil, to the approximations made in the computer calculation, or to errors of measurement.

Returning to the normal operating method for the vibrating coil magnetometer, we now have an expression for the flux in each pick-up coil. Using this expression in the equation for V_1, we find

$$V_1(x,t) = \sqrt{2}A_1(\omega_1/\omega_2)\cos\omega_1 t \; [-\partial/\partial x(V_2(x)_{rms})]$$

The maximum in the rms voltage obtained from the above equation will occur when the midpoint of the vibration is near the maximum of $|\partial/\partial x(V_2(x)_{rms}|$. By vibrating parallel to the pole faces of the magnet one can locate the pick-up coils at this maximum. Also, with an amplitude of vibration of 1.27 cm the change in flux through the coils in one-half cycle can be 75% of the total flux available.

The dimensions of the pick-up coils with their resistance and inductance are given in Figure 3. Each coil contains 23,452 turns of forty gauge copper wire embedded in epoxy. The coils vibrate at 15 Hz which is far below the 5100 Hz resonance frequency of the coils. Figure 4 shows a picture of the pick-up coils in their plastic holder.

A drawing of the mechanical vibrator is shown in Figure 5. It is very important to maintain a stable path for the vibration cycle. A shift in this path relative to the magnet during a

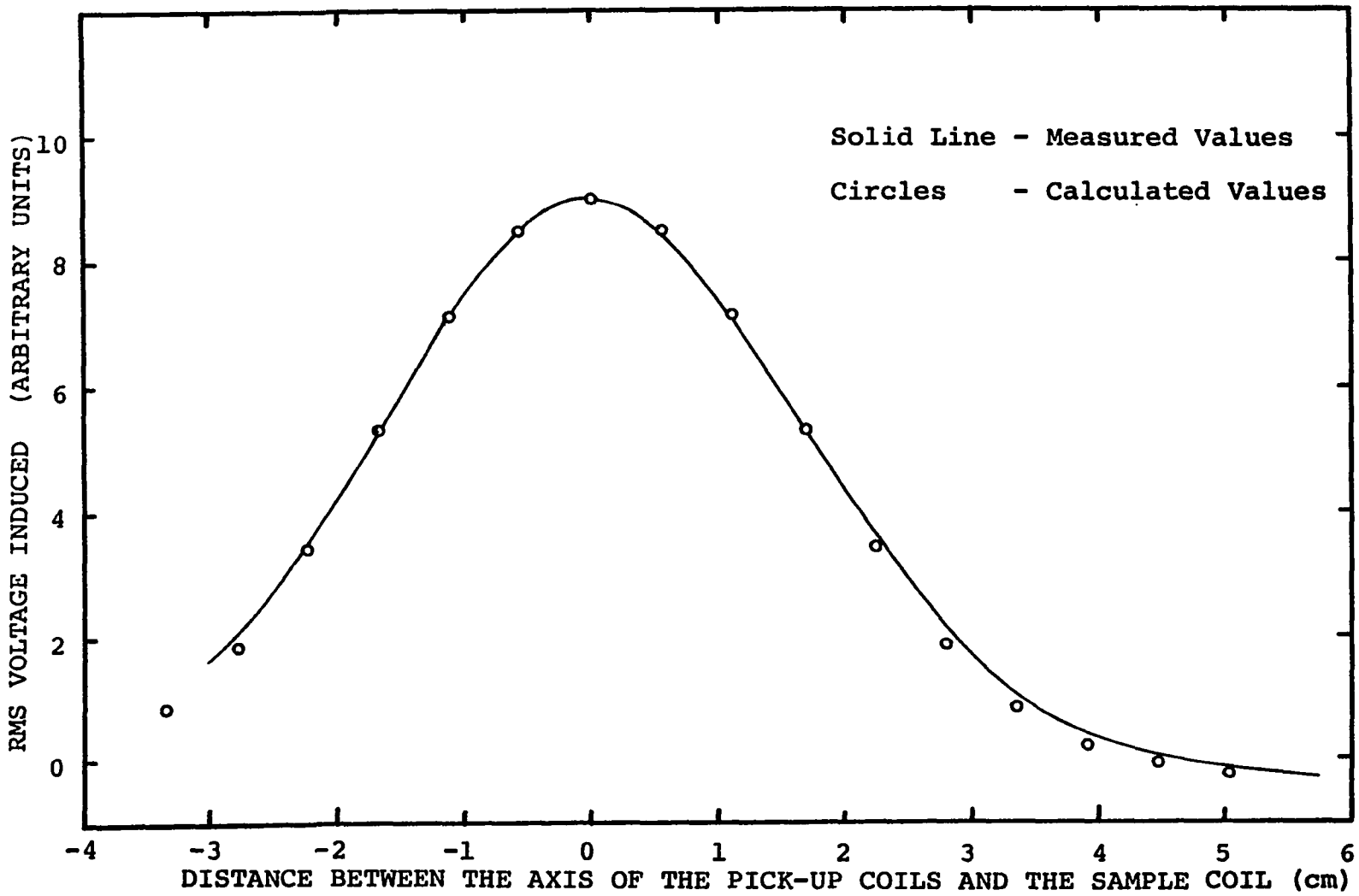

Figure 2. Induced Voltage as a Function of Position

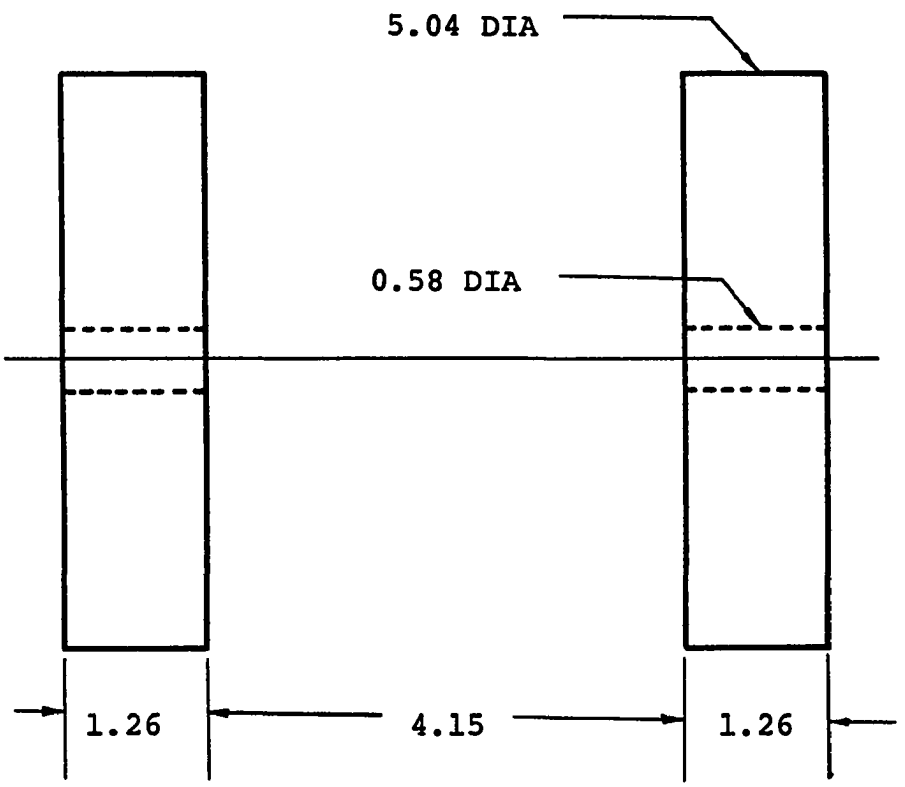

Figure 3. Dimensions and Electrical Parameters of the Pick-up Coils. The coils, which are encapsulated in epoxy, are held in the above configuration by a plastic form. All dimensions are given in centimeters. The resistance in ohms and the inductance in henries are 7,410 ± ½% and 8.43 ± ½% for each coil respectively.

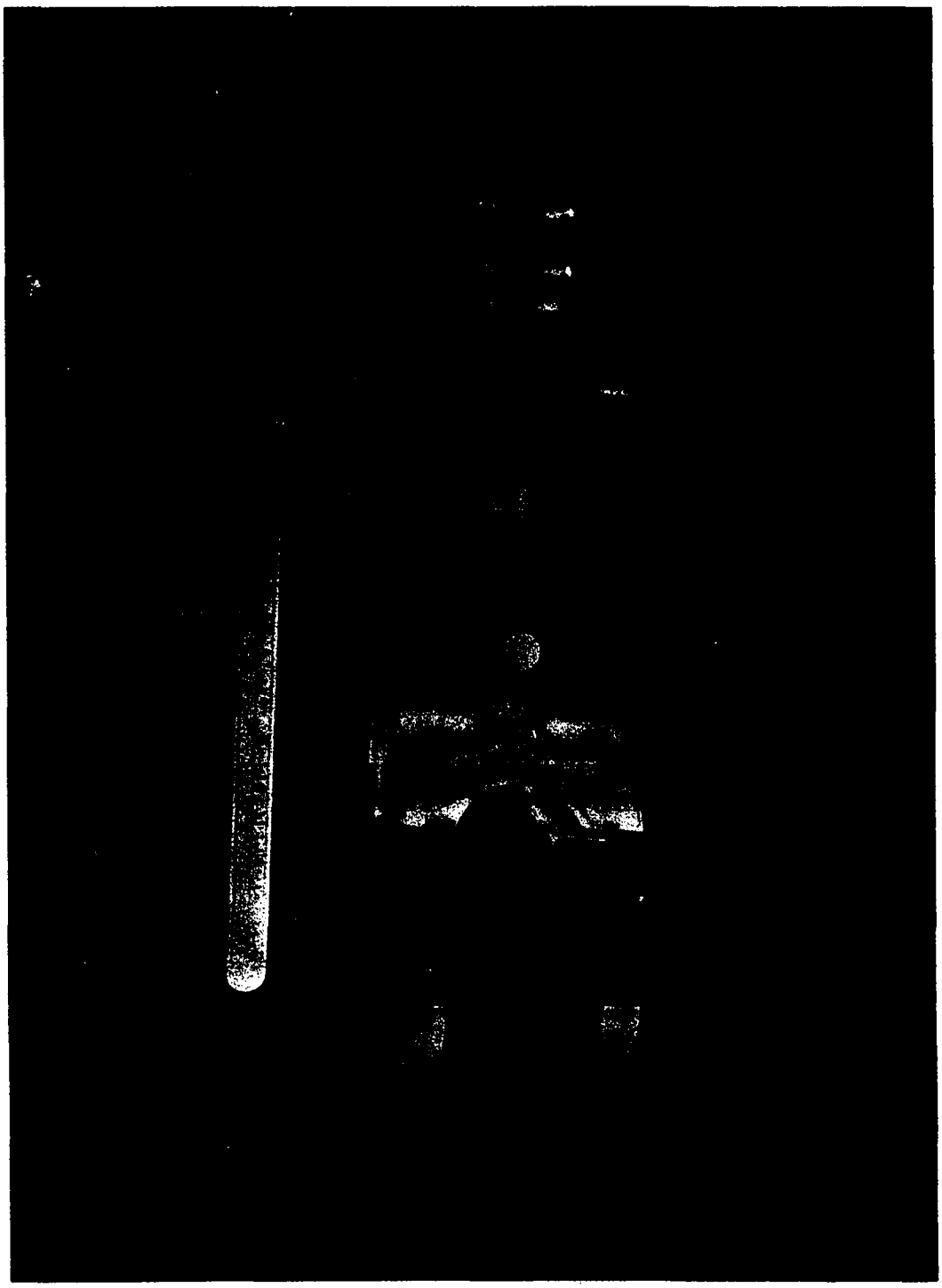

Figure 4. Pick-up Coils of the Magnetometer in Their Plastic Holder.

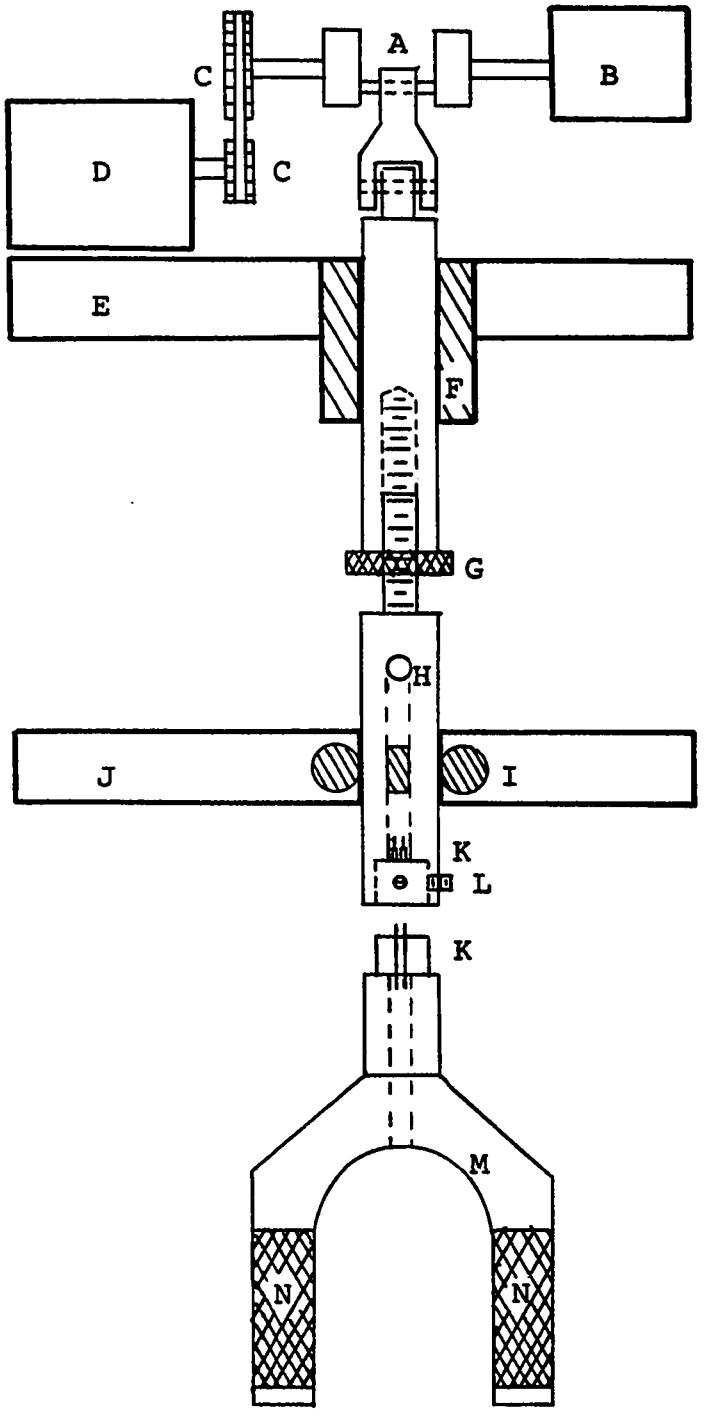

A. Offset Shaft

B. Generator to Provide Lock-in Frequency

C. Toothed Pulley

D. Synchronous Motor

E. Mounting Plate

F. Linear Ball Bearing

G. Locking Nut

H. Outlet for Pick-up Coil Leads

I. Ball Bearing, 4 ea.

J. Guide Plate

K. Four-pin Connector for Pick-up Coil Leads

L. Set Screw, 2 ea.

M. Coil Holder

N. Pick-up Coil

Figure 5. Vibration System.

measurement creates a non-correctable error signal in the pick-up coils. The frequency of vibration is chosen by using a synchronous motor and toothed pulleys. Pictures of the vibrator are shown in Figures 6 and 7.

The AC voltage induced in the pick-up coils is converted to a proportional DC voltage by a phase sensitivity detector (lock-in amplifier). The lock-in reference frequency is derived from the generator shown in Figure 5. To increase the range and accuracy of the magnetization measurement, the lock-in amplifier is used as a null device. This is accomplished by adding a pair of balance coils of 500 turns each. These balance coils are placed symmetrically on each side of the sample inside the pick-up coils. The balance coils are pictured in Figure 8 on the outside of the dewar which contains the sample. The DC current in the balance coils is adjusted until the lock-in amplifier shows that its signal is equal and opposite to that caused by the sample. The measurement of the magnetization is now related to a DC current. This measurement is not effected by the resistance of the pick-up coils or the gain of the lock-in. A schematic of the electronics is shown in Figure 9.

The small coil used to study the magnetometer is also used to calibrate it. The magnetic dipole moment m_2 of a coil is

$$m_2 = n\pi a^2 (I_2/10)$$

where

n = number of turns,

a = radius of a turn in cm., and

I_2 = current in amperes.

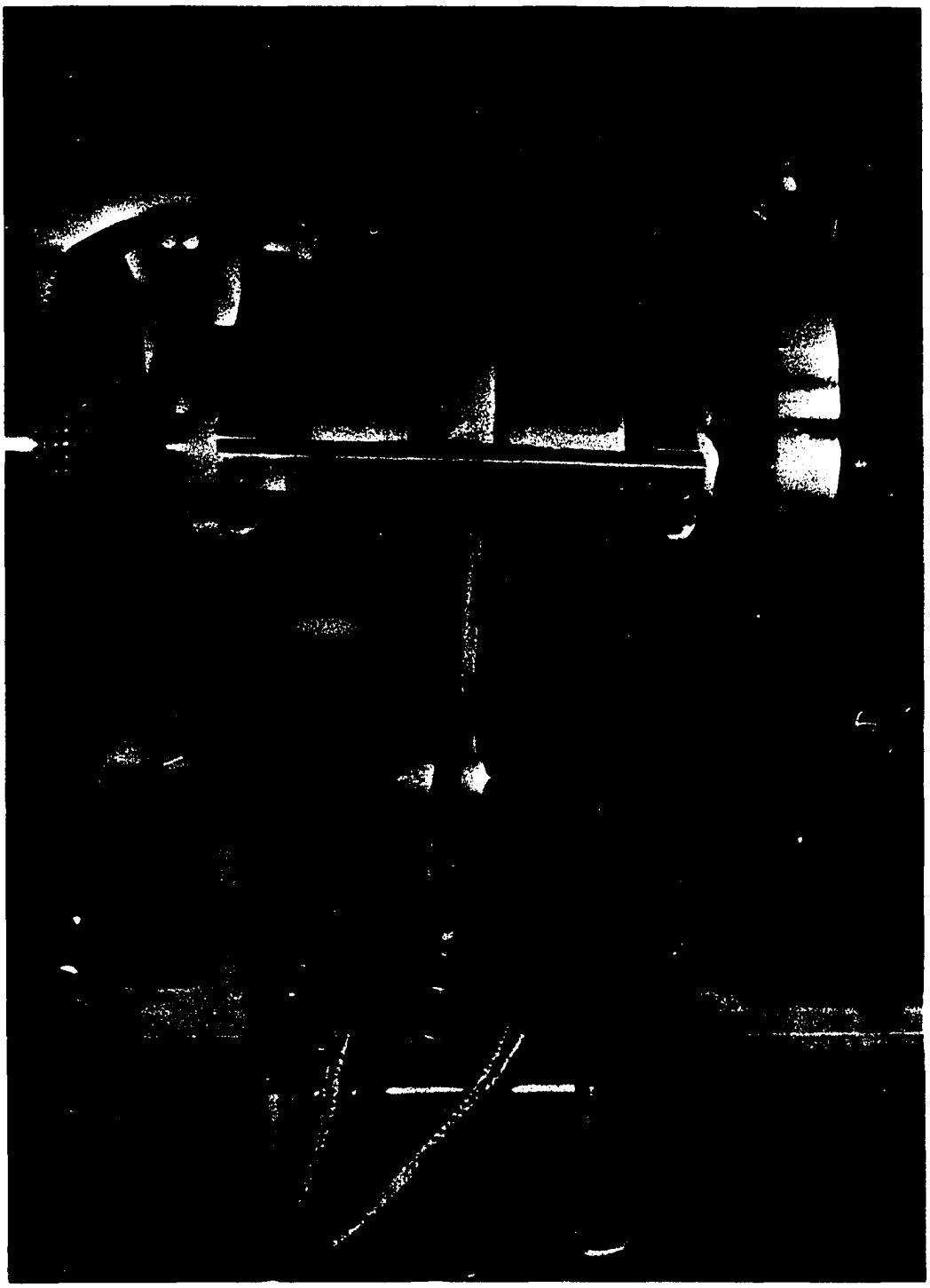

Figure 6. Drive Mechanism with Synchronous Motor for Vibrating the Pick-up Coils.

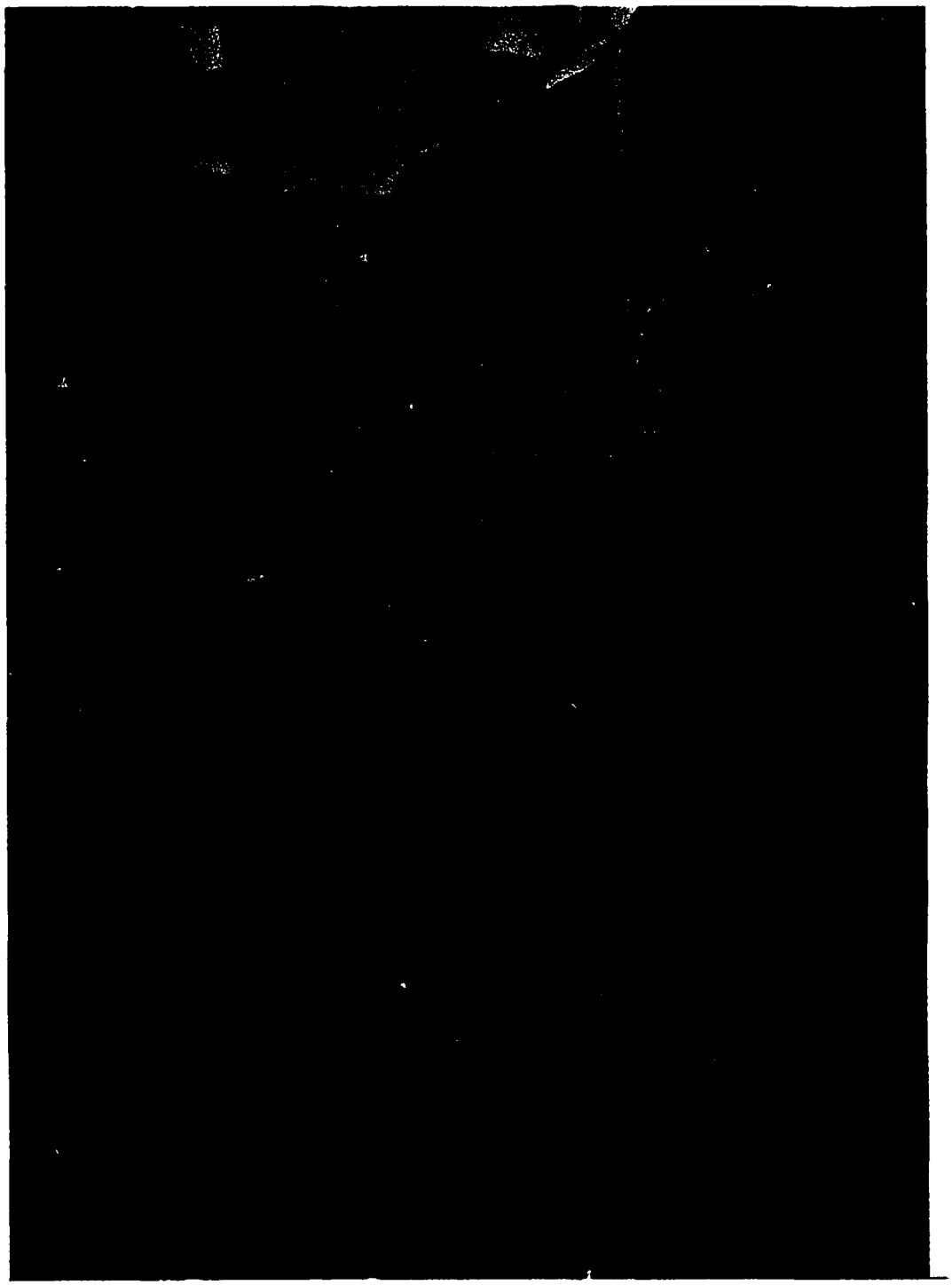

Figure 7. Drive Shaft with Guides for the Pick-up Coils.

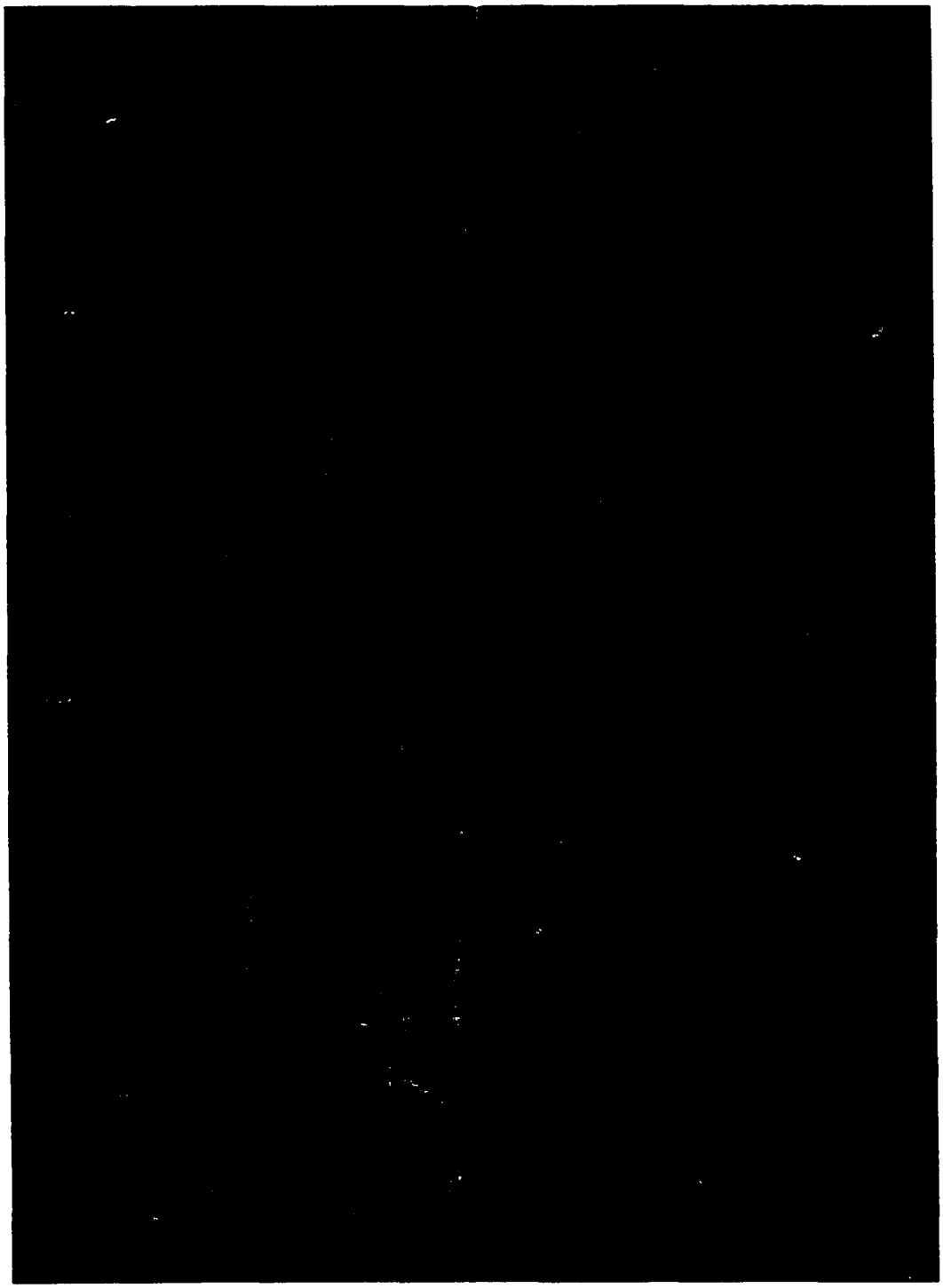

Figure 8. Balance Coils Mounted on the Sample Dewar.

Null Detection Circuit

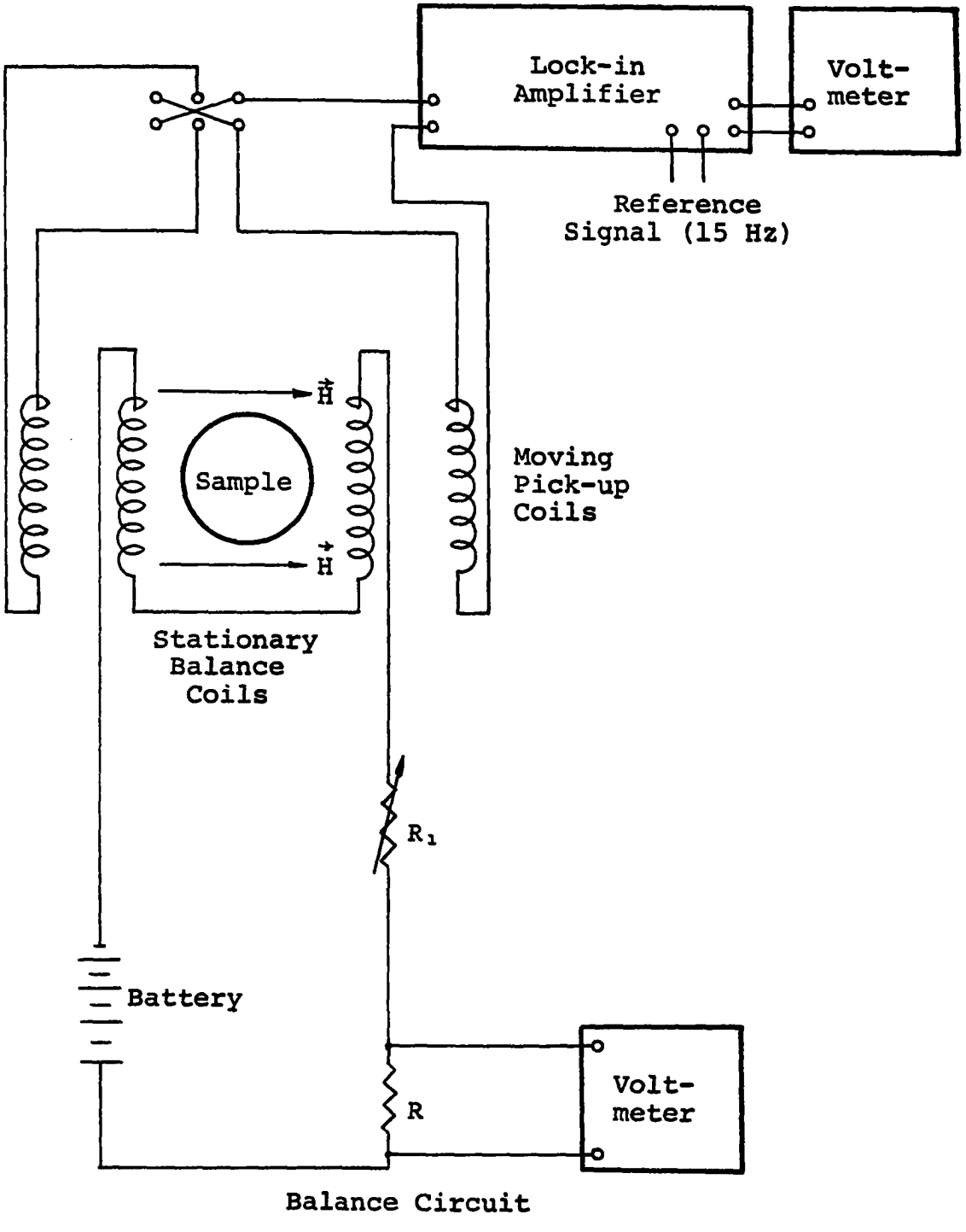

Figure 9. Electronic Circuits

The calibration coil has two layers of 127 turns each with radii of 0.314 and 0.324 cm respectively. For m_2 we have

$$m_2 = 8.12\ I_2 \text{ gauss-cm}^3$$

The quadrupole field of the coil limits the accuracy of the calibration since it can be as large of 2% of the dipole field in the vicinity of the pick-up coils.

A current I_1 in the balance coils can now be found which nulls the signal created by the calibration coil. This null current in amperes is

$$I_1 = (0.003970 \pm 0.000004)I_2$$

The equivalent magnetic moment m_1 corresponding to the null current in the balance coils is

$$m_1 = 2045\ I_1 \text{ gauss-cm}^3$$

The proportionality between I_1 and I_2 is independent of the applied magnetic field. The magnitude of the magnetic image in the pole faces of the electromagnet is, therefore, linearly proportional to its magnetic dipole source over the range of magnetic fields used. The sample and balance coils may have different magnetic images due to their different spatial configurations. This will not affect the precision of the measurements, but it could affect the calibration by 1%.[15] The calibration error for the absolute magnetization is 3%.

Magnetic Field

The magnetic field is created by a 6 inch magnet shown in Figure 10. Because the separation of the poles pieces is fixed, ring shims are used to increase the field homogeneity between the pole pieces. The magnetic field is calibrated by using the

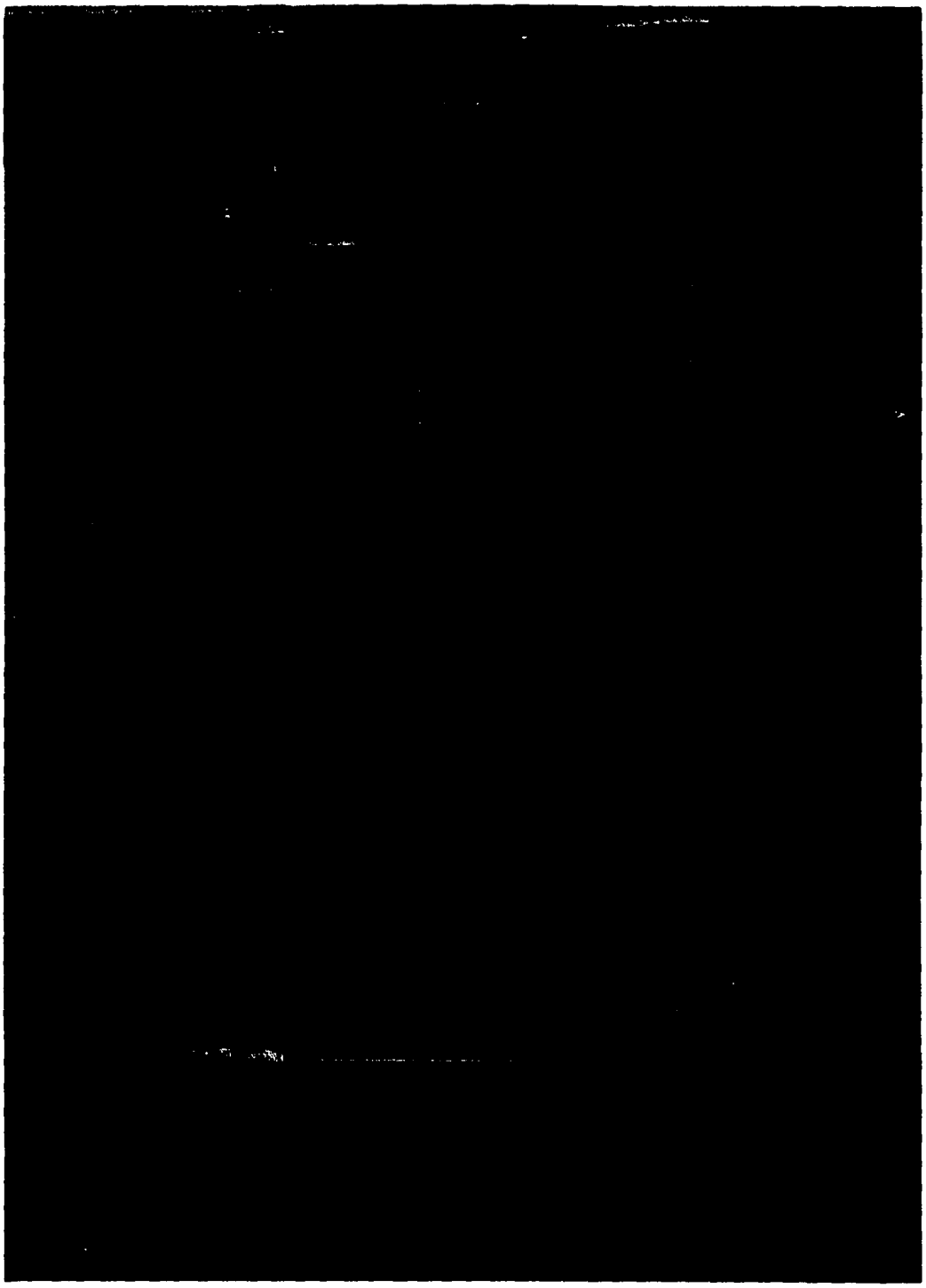

Figure 10. Magnet with the Sample Dewar in Place.

nuclear magnetic resonance of protons in a $CuSO_4$ solution.[16] The current in the magnet for each known field is determined from the voltage developed across a fixed resistor in series with the magnet. This current is always approached from above the desired value to insure that the same part of the hysteresis curve is retraced. The maximum attainable field using the regulated power supply is 5 kilogauss and this field has an uncertainty of less than 3 gauss.

Temperature

The temperature of the sample is controlled by placing the sample holder inside a dewar. Antifreeze from a constant temperature bath is circulated around the sample holder. The holder and dewar are shown in Figure 11.

The temperature is measured by two methods. First, a thermistor is located at one end of the sample holder as shown in Figure 11. The temperature difference between the thermistor and the sample is very small because they are in close proximity in the same beryllium-copper holder. The thermistor detects changes in temperature as small as 0.01 K. Second, a copper-constantan thermocouple is placed in the fluid circulating around the sample holder. With a Leeds and Northrup Type K potentiometer the temperature is measured to a precision of 0.03 K. The accuracy of the thermocouple temperature is 0.2 K after calibration.[17]

Pressure

The sample holder is made from a 98% copper-2% beryllium alloy. This alloy is non-magnetic except for its cobalt impurities.

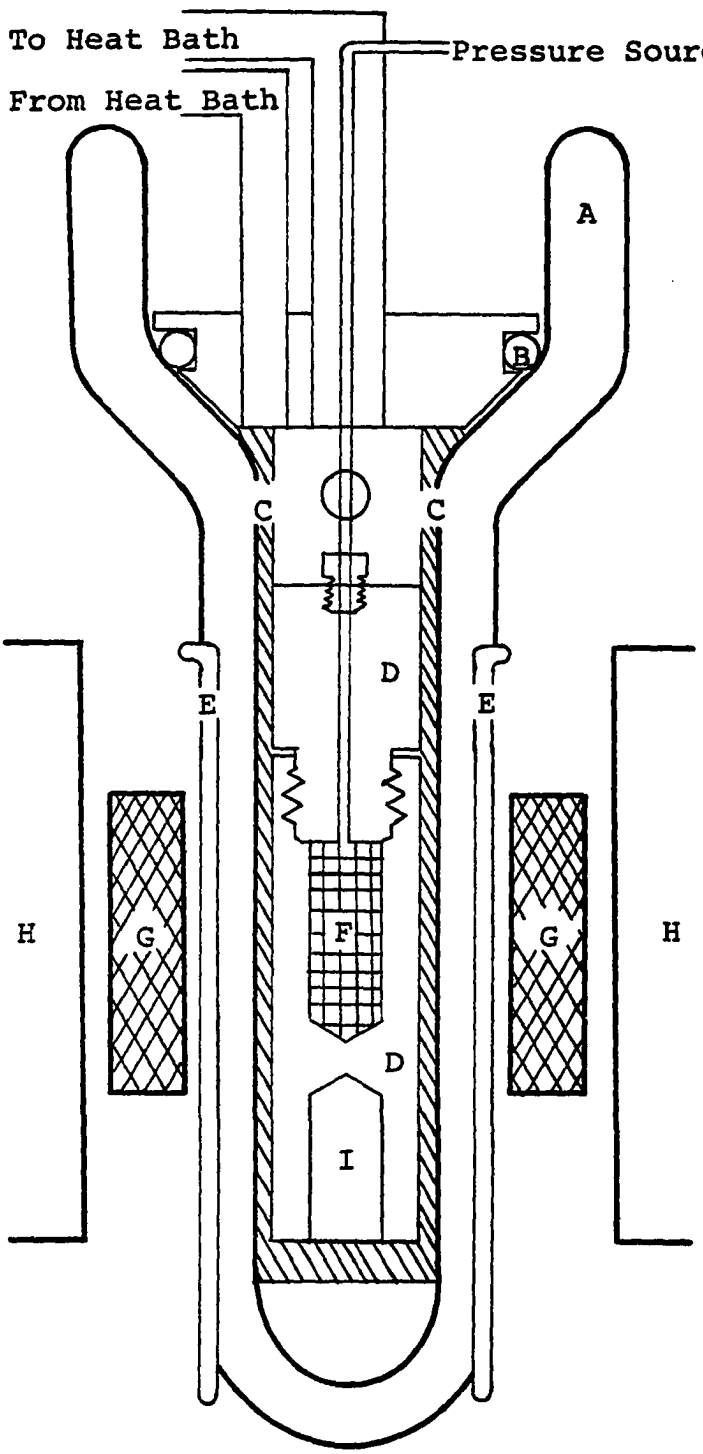

A. Dewar
B. O-ring
C. Seals
D. Pressure Bomb
E. Balance Coils
F. Sample
G. Pick-up Coils
H. Magnet
I. Thermistor Well

Figure 11. Pressure Bomb Inside the Dewar. Fluid from the heat bath flows behind the bomb, then up in front and out.

The sample holder is shown in Figure 12. It is 2.54 cm in diameter by 8.90 cm long. The sample chamber is 3.81 cm long and 1.42 cm in diameter.

The pressure is applied by hydraulic fluid from a jack pump. The maximum pressure attainable is 3 kilobars. The Bourdon gauge used to measure the pressure is calibrated at the low part of the range by using the known vapor pressure over liquid CO_2 at 0°C and 31°C. The Bourdon gauge is accurate to ± 1/2% of full scale or ± 0.02 kilobar.

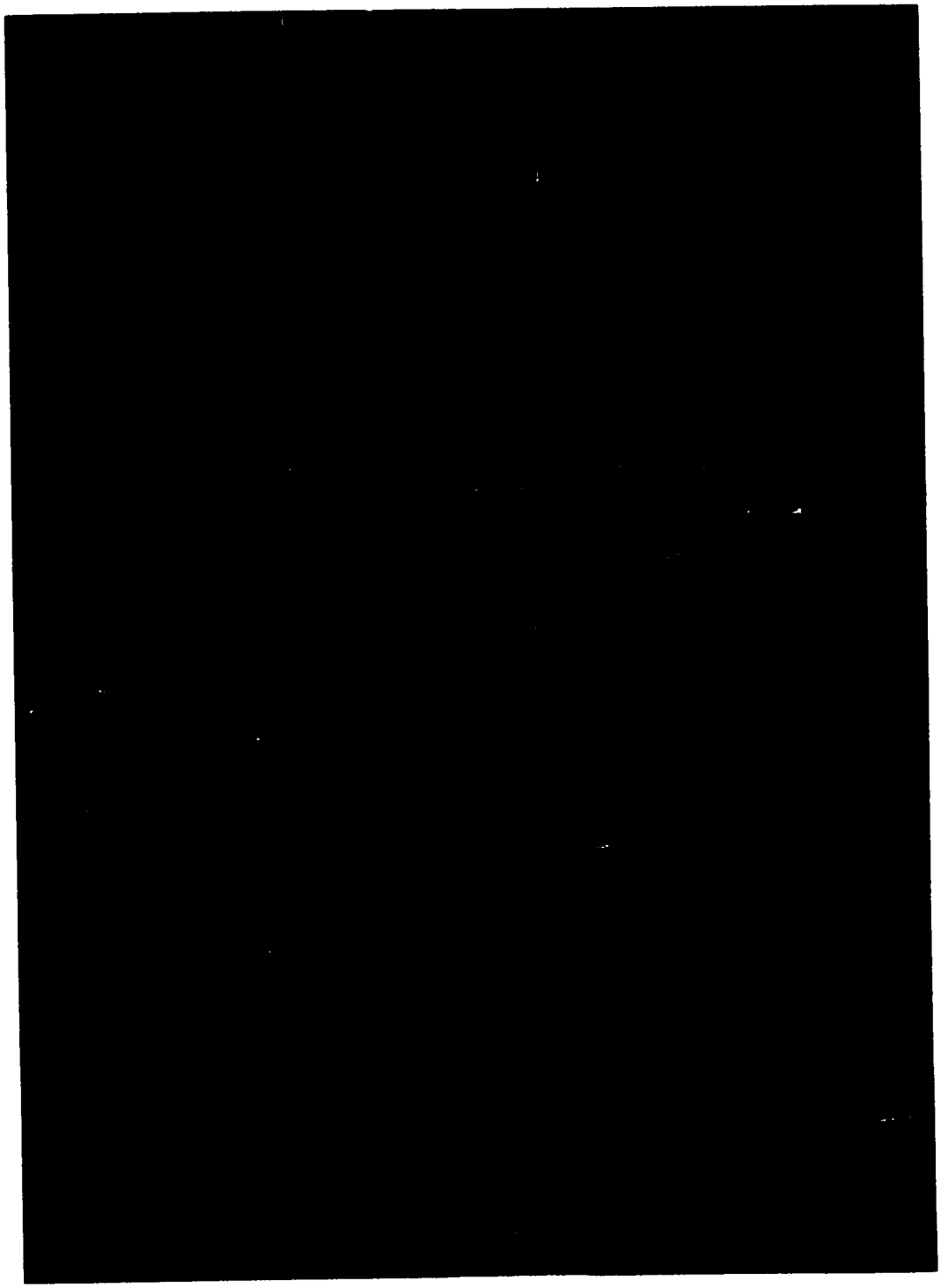

Figure 12. Beryllium-Copper Pressure Bomb with Seals.

CHAPTER III

SAMPLE PREPARATION

Single crystals of iron borate can be grown in a slowly cooled flux[18,19] but the crystals are hexagonal plates typically only 5 mm across and 0.2 mm thick. These single crystals are too small to be measured in the magnetometer. Therefore, a powdered sample has to be used.

An outline for making $FeBO_3$ powder was published in 1968 by J. C. Joubert, T. Shirk, W. B. White, and Rustum Roy.[12] They took 1:2.1 molar quantities of Fe_2O_3 and H_3BO_3 and reacted them in a furnace to get $FeBO_3$. The main contaminant in the reaction product is Fe_3BO_6. To get a better product it was decided to use a large excess of B_2O_3 as is done to get single crystals in the flux method. The work of T. A. Grigor'eva and A. V. Nikolaev[20] in the Fe_2O_3-B_2O_3-H_2O system also indicates that excess B_2O_3 would produce purer $FeBO_3$.

The detailed method for making and analyzing the sample is given in Appendix II. In general, the method involves ball milling B_2O_3 and then adding sufficient Fe_2O_3 to give a 5.6 B_2O_3-Fe_2O_3 ratio. The mixture is again ball milled, then dried. Next the mixture is placed in a quartz tube, which is evacuated, sealed, and heated 36 hours at 600°C followed by 120 hours at 800°C. Excess B_2O_3 is removed from the reaction product by washing in hot distilled

water. Magnetic material is separated from quartz particles by using a magnet. Microscopic examination shows that the sample consists of platelets which generally range from 1 to 5 microns in diameter. Very small platelets are removed by decanting the wash water while it still had a green tint.

A sample is analyzed by dissolving it in an acid and then titrating it to obtain the weight percentage of iron and boron. Oxygen is calculated by the difference. The result is shown in Table I.

Table I. Chemical Analysis of $FeBO_3$

Element	Weight Percentage
Fe	48.1 ± 0.2
B	8.9 ± 0.6
O	43.0

The analysis gives $FeB_{0.96}O_{3.13}$ but $FeBO_3$ is included within the experimental error.

An X-ray scan of the above sample using Cu Kα radiation is made using a Norelco Diffractometer. Only $FeBO_3$ diffraction peaks are present. The half-width of the peaks are equal to the instrument broadening, thus showing that few crystals have dimensions less than 1000 A. A well formed contaminant could have been seen in the diffraction pattern if present in a concentration of 10%. Overall the sample contained well formed platelets of iron borate of good purity.

CHAPTER IV

EXPERIMENTAL PROCEDURE

Experimental Technique

A measurement is divided into two basic steps. First, the independent variables in the order of temperature, magnetic field, and pressure are set and measured. Then the resultant signal from the magnetometer is obtained and reduced to a magnetization.

The magnet, the pick-up coils, the balance coils, and the sample have an optimum relative position for a reproducible magnetometer signal. The sample coordinate system as defined in Chapter II will be used to describe this relative position. We have the x axis horizontal and perpendicular to the applied magnetic field, the y axis vertical and perpendicular to the magnetic field, and the z axis parallel to the field.

The vibrating mechanism for the pick-up coils is rigidly attached to a wall. Therefore the magnet, which is on rollers, is moved. When the magnet is correctly positioned the pick-up coils are parallel to the faces of the pole pieces and vibrating about the center of the magnetic field. The curvature of the magnetic field (which increases as the field becomes larger) induces a signal with its main component at the second harmonic of the vibrating frequency. The lock-in amplifier suppresses this harmonic. However, the smaller third harmonic of this signal is amplified by the lock-in and

determines a null signal level. The pick-up coils are connected so that they can be switched either in series or in opposition. The magnet is moved until the signal in the pick-up coils is minimized for both configurations. The largest source of noise is the shift in the null signal. This shift occurs when the position of the pick-up coils changes with respect to the magnetic field and is proportional to the curvature of the magnetic field. Therefore stability of the vibrating coils is very important.

The balance coils are inserted and a dipole field is created with DC current. The coils are moved in the x direction until the signal from the series connected pick-up coils is maximized. The balance coils are designed so that movement in the y direction causes no change in the signal. The pick-up coils are now connected in opposition. The balance coils are moved in the z direction until an equal signal is induced in each pick-up coil, resulting in a null. The sample is now positioned independently using the same procedure as for the balance coils. Additionally both the balance coils and the sample are moved in the y direction until the sample induces a maximum signal with the pick-up coils connected in series.

The magnet, pick-up coils, balance coils, and sample are now in the correct relative position. Since the position of the balance coils and sample causes the signal to have an extremum, small shifts in their position cause little change in the magnitude of the signal.

With the sample in position the heat bath is adjusted until the desired temperature at the sample is achieved as determined by the thermocouple. The thermistor is used to return precisely to this temperature. The magnetic field and pressure are set as desired.

The current in the balance coils that creates a signal equivalent to that of the sample is determined as follows:

1. An initial null is established from the lock-in amplifier with no sample in the magnetometer and no current in the balance coils.
2. The sample is placed between the pick-up coils and the correct fluid flow pattern from the heat bath is established around the sample. The thermistor in the end of the sample holder indicates when the desired temperature is precisely reached. Current in the balance coils is now adjusted until a trial null is found. This trial null will have a lock-in voltage V_1 close to the initial null. The current I_b in the balance coils is measured.
3. The sample is removed and the current in the coils is turned off. The true lock-in amplifier null V_o is immediately measured. (Steps 2 and 3 are repeated at least once. I_b is held constant in all replicate measurements.)
4. A current of 1 μA in the balance coils causes the lock-in voltage to decrease 3.8 mV. The current I_s which creates a signal equivalent to that of the sample is

$$I_s = I_b + (2.6\times10^{-4}/n)\sum_{1}^{n}(V_1 - V_o)_i \pm (5\times10^{-4}I_s + 2.6\times10^{-8} + 10^{-9}H/\sqrt{n})$$

where current is to be expressed in amperes, voltage in volts, and magnetic field in oersteds. The number of times the measurement is replicated is n. The first two terms in the error are determined from the 0.05% accuracy of the voltmeter and its least count. The third

error term, caused by the curvature of the applied magnetic field, usually dominates. As expected, this error is proportional to the applied field. Its value decreases by $\sqrt{n}$ on replication because the error is random. (Additional error introduced when pressure is applied will be discussed later.) Since this current is proportional to the magnetization its percent error mainly determines the precision of the relative magnetization.

Sample Holder

Because the sample holder contains cobalt it has a significant magnetization. This magnetization is independent of the applied pressure but is slightly dependent on the temperature and strongly dependent on the applied magnetic field. A strong magnetic sample is placed in the holder and its signal is maximized to determine the correct position for the holder. Then the sample is removed and the holder positioned as before.

Its magnetization is measured at 20°C, 60°C, and 100°C. The results are shown in Figure 13. The magnetization at intermediate temperatures is obtained by linear interpolation.

Sample Size Effect

After the sample holder is partially filled with hydraulic fluid 10.19 grams of $FeBO_3$ are added. Next filter paper disks are forced into the holder compacting the sample. The sample is 1.41 cm in diameter by 3.3 cm long.

The magnetometer is calibrated with a coil having its long axis parallel to the applied magnetic field and not extending outside

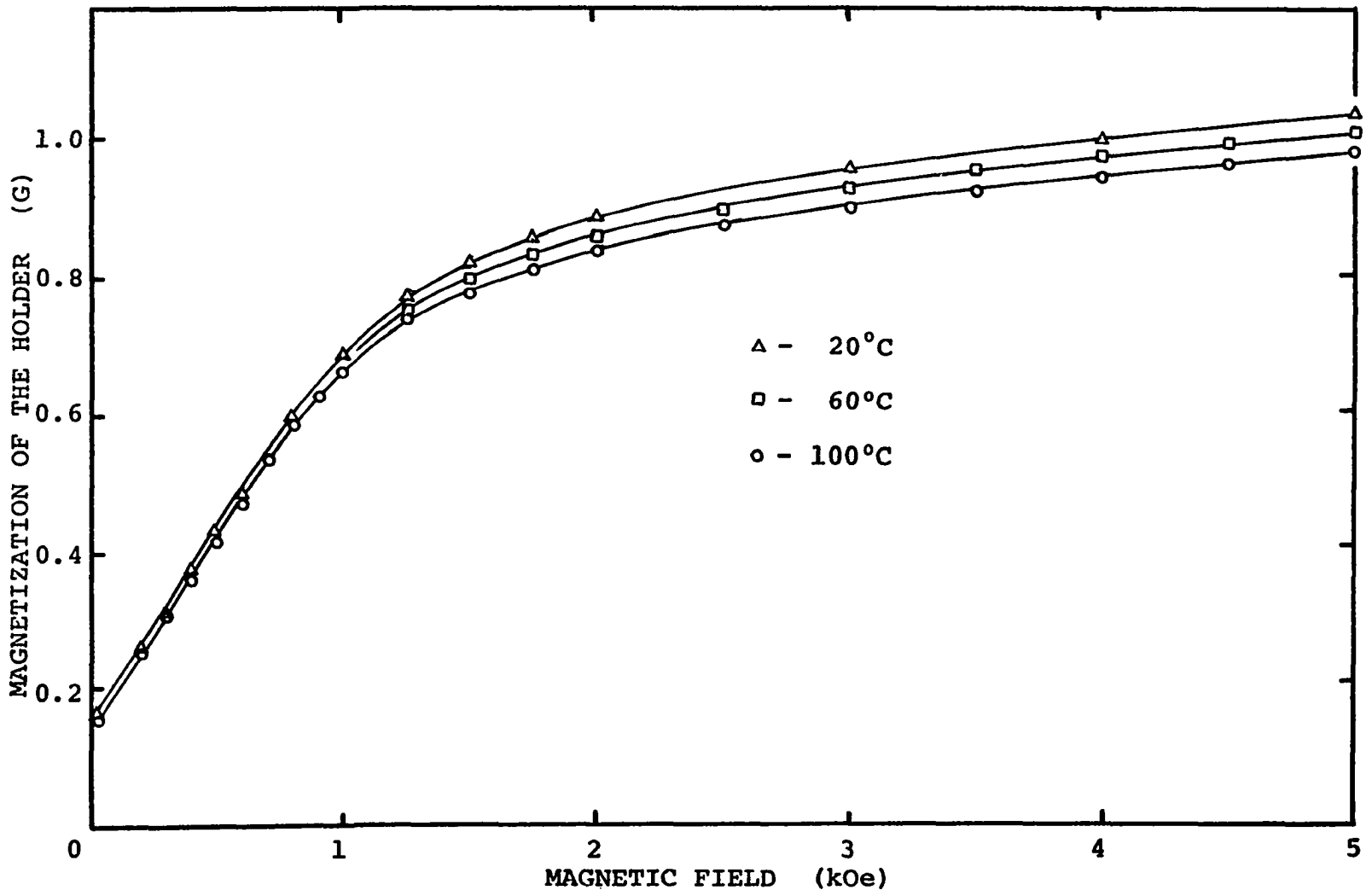

Figure 13. Sample Holder Magnetization as a Function of Magnetic Field

the most sensitive region of the pick-up coils. The sample, on the other hand, has its long axis perpendicular to the applied field and its length does extend into the region of reduced sensitivity. To correct the signal for the reduced sensitivity the cylindrical sample and sample holder are mathematically divided into thirteen thin disks and the relative sensitivity to each disk determined. The thickness of each disk is chosen to be 0.25 cm. The small signal from the sample holder is assumed to have the same spatial distribution as the sample. The signal is measured every 0.254 cm as the sample is vertically lowered into the magnetometer. Using the differences in these signals one can calculate the contribution to the signal from one disk as a function of position. The results are shown in Figure 14.

The signal from a 0.254 cm disk at the center of the pick-up coils is the peak value in Figure 14. The signal from the other disks in the sample will drop as indicated in the curve of Figure 14. If all of the disks were located in the sensitive central region, then the sample signal would be thirteen times the peak value minus the sample holder signal. This calculated signal is equivalent to 5370 μA in the balance coils. The actual signal is 4880 μA. Therefore, (5370 - 4880)/4880, or 10%, must be added to the measured signal to correct for the reduced sensitivity of the pick-up coils to the magnetization located at each end of the sample. Now with this correction to the sample signal, the calibration constant applies. Because of the approximations involved we estimate the error in this correction to be of the order of the ratio of sample holder signal to the sample signal. The ratio is 0.2. This error

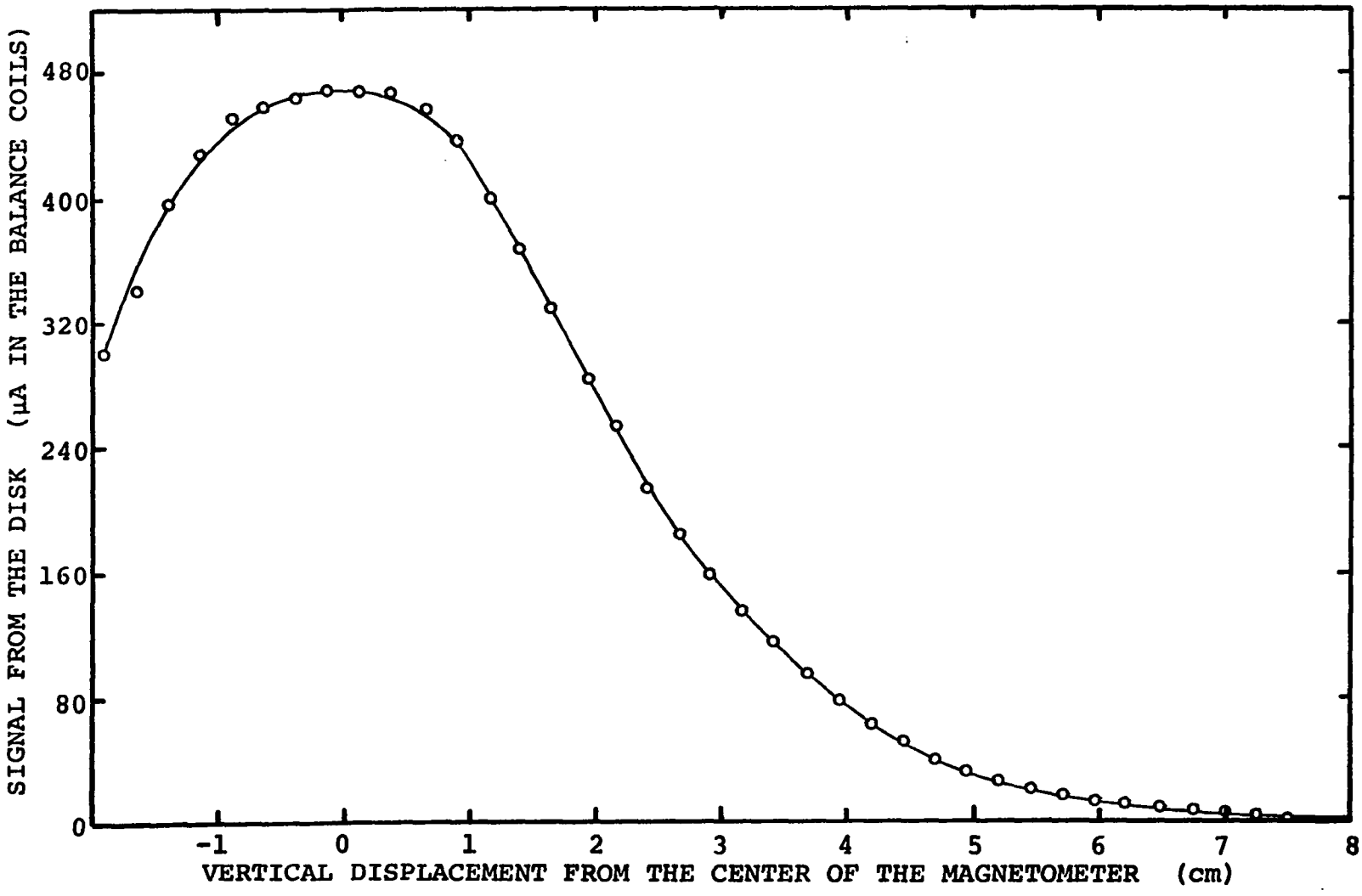

Figure 14. Signal of a Disk as a Function of Position

then adds 0.2 times 10% or 2% to the uncertainty in the absolute magnetization. With an error of 3% in the calibration constant, ½% in the sample weight, and at least 0.1% in the relative magnetization (of both the sample and holder), the total uncertainty in the absolute magnetization is typically 6%. However, if we are only interested in the relative magnetization of the sample, then its precision can be as small as 0.1%.

Sample Compression Correction

When pressure is applied the sample decreases in length. This change in length is twice the distance the sample must be raised to recenter it. The sample is centered when sample displacements of 0.254 cm both upward and downward cause the same decrease in the signal. The signal from the sample holder is insensitive to these small vertical displacements. The sample compression is non-linear with pressure and shows hysteresis. Above the Curie temperature the sample signal is so small that it cannot be used for positioning. In this case the sample is first centered below T_C. Then above T_C, a previously established centering pattern that corrects for the pressure induced sample displacement is automatically followed.

The increase in the signal due solely to the shorter sample is proportional to the magnetization and, to the first order, proportional to the change in sample length. This proportionality constant can be found using the data in Figure 14. The signal I_S from a sample of length L divided into thirteen disks is

$$I_S(L) = k\rho_o \sum_{1}^{13} Y_i$$

where

k = proportionality constant,

ρ_o = density of the sample when it is of length L, and

Y_i = signal from the i-th disk.

If the sample is compressed by a length ΔL and recentered, the signal is

$$I_S(L-\Delta L) = k\rho[\sum_1^{13} Y_i - 6.5(\Delta L/L)(Y_1+Y_{13})]$$

where

ρ = density of the sample when it is of length $L - \Delta L$. Since the mass and diameter of the sample are constant, we have

$$\rho = \rho_o L/(L-\Delta L)$$
$$\simeq \rho_o(1+\Delta L/L).$$

The relative change in the signal is

$$\Delta I_S/I_S = [I_S(L-\Delta L) - I_S(L)]/I_S(L)$$

$$= \frac{k\rho_o(1+\Delta L/L)[\sum_1^{13} Y_i - 6.5(\Delta L/L)(Y_1+Y_{13})] - k\rho_o\sum_1^{13} Y_i}{k\rho_o\sum_1^{13} Y_i}$$

To the first order in $\Delta L/L$ we get

$$\Delta I_S/I_S = (\Delta L/L)[1 - 6.5(Y_1+Y_{13})/\sum_1^{13} Y_i].$$

Using the values for Y_i derived from Figure 14, we find

$$\Delta I_S = 0.20\ I_S\ \Delta L/L.$$

For a pressure of 3 kilobar $\Delta L/L$ was typically 0.04. A 20% error in the above calculation and a 15% error in the measurement of ΔL is possible. These errors would add 0.3% uncertainity to the relative magnetization when the pressure is varied. This additional error is only important below the Curie temperature where the magnetization is large and the pressure effect, small.

Demagnetizing Field Correction

The magnetization at the surface of the sample creates an internal demagnetizing field which opposes the applied field. The cylindrical sample is approximated by a prolate ellipsoid with a long axis to short axis ratio of 2.3. Then the demagnetizing field parallel to the short axis is approximately 1.7 π times the magnetization.[21]

The magnetization M of the sample (with correction for the sample size effect) is

$$M = \rho m_1/w$$

$$= (2045)(1.10)(\rho/w) I_S$$

$$= 940\ I_S \text{ gauss}$$

where

m_1 = magnetic moment of the sample,

w = mass of the sample in grams,

I_S = current in balance coils in amperes, and

ρ = density of $FeBO_3$, 4.26 gm/cm^3.

The demagnetizing field H_d becomes

$$H_d = 1.7 \pi M$$

$$= 5 (10^3) I_s \text{ Oe.}$$

This demagnetizing field is substracted from the applied magnetic field to get the field inside the sample. Inside a cylinder the demagnetizing field is not a constant, but the calculated demagnetizing field should be a good approximation. More importantly, the demagnetizing field is always less than a twentieth of the applied field and normally a hundredth to a thousandth of it. Thus an error of 20% in correcting for the demagnetizing field makes no difference in the final results and an error of 100% makes little difference.

The Data

The data is recorded in Appendix III. The temperature ranges from 20°C to 100°C with emphasis placed near T_C. The applied magnetic field, which varies between 39 and 5000 gauss, is corrected for the demagnetizing field of the sample. The hydrostatic pressure is given at 0,1,2, or 3 kilobar. After correcting for the sample holder, sample size effect, and sample compression, the signal is multiplied by the calibration factor to give magnetization in gauss.

CHAPTER V

THEORY

Weak Ferromagnetism

Dzialoshinskii[13] developed a theory of 'weak' ferromagnetism based on Landau's theory of second order phase transitions. Applying group theory to the magnetic symmetry of rhombohedral ($R\bar{3}c$) crystals he obtained the possible lower order magnetic terms in the Gibbs free energy. By minimizing this free energy with respect to the magnetic vectors, equations for the magnetization as a function of temperature T, pressure p, and magnetic field $\vec{H}$ are obtained. Dzialoshinskii used his theory to explain many of the magnetic properties of α-Fe_2O_3. Iron borate, also has $R\bar{3}c$ symmetry and, therefore, the 'weak' ferromagnetism theory of Dzialoshinskii will be applied.

A crystal of $FeBO_3$ is divided into two sublattices with magnetization $\vec{M}_1$ and $\vec{M}_2$ as shown in Figure 15. With the coordinate system given in the figure, the lower order terms in Dzialoshinskii's equation for free energy near the Curie temperature are

$$\tilde{\Phi} = \Phi_o + 2M_o[\tfrac{1}{2}A\lambda^2 + \tfrac{1}{2}B\mu^2 + \tfrac{1}{4}C\lambda^4 + \tfrac{1}{2}a\lambda_z^2 - D(\lambda_y\mu_x - \lambda_x\mu_y) - \vec{\mu}\cdot\vec{H}] \quad (1)$$

where

$\tilde{\Phi}(p,T,\vec{H})$ = Gibbs free energy as a function of pressure, temperature and magnetic field,

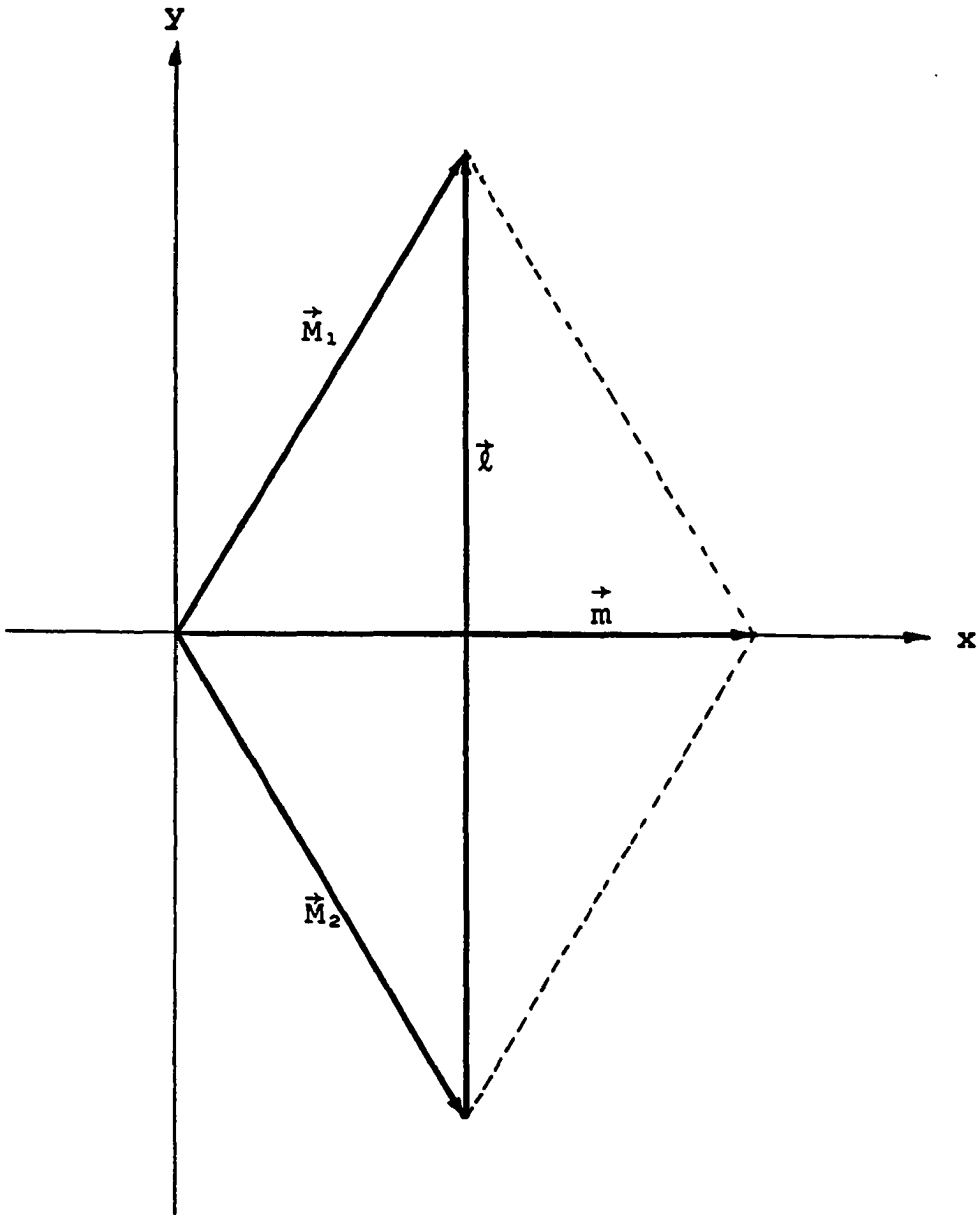

Figure 15. Coordinate System for Single Crystals. The z axis, out of the plane of the paper, is parallel to the [111] direction of the rhombohedral unit cell. The x axis, along a two fold symmetry axis, and the y axis define a basal plane.

$\Phi_o(p,T)$ = non-magnetic part of the free energy,

M_o = magnitude of the magnetization at zero degrees Kelvin for each of the sublattices.

$\vec{\ell} = \vec{M}_1 - \vec{M}_2$ is the antiferromagnetic vector,

$\vec{m} = \vec{M}_1 + \vec{M}_2$ is the ferromagnetic vector of the magnetization,

$\lambda(p,T,\vec{H}) = \vec{\ell}/2M_o$ is proportional to the antiferromagnetic moment in the crystal and is used as the order parameter since it varies from zero to almost one, and

$\vec{\mu}(p,T,\vec{H}) = \vec{m}/2M_o$ is proportional to the ferromagnetic moment of the crystal.

A(p,T), B(p,T), and C(p,T) are coefficients characterizing the isotropic superexchange interaction. As written, they are expressed in magnetic field units. Note that the associated energy terms ($A\vec{\lambda}\cdot\vec{\lambda}$, etc.) are independent of the direction of $\vec{\lambda}$ and $\vec{\mu}$.

a(p,T) and D(p,T) are coefficients characterizing the magnetic anisotropy in the crystal. 'D' is called the Dzialoshinskii - Moriya constant.

Only combinations of vectors resulting in a scalar are found in Equation (1) because it is an expansion of energy in terms of vectors.

Dzialoshinskii believes that the a(p,T) and D(p,T) interactions arise from relativistic spin-lattic interactions.[13] Toru Moriya[22] derived an expression for the Dzialoshinskii interaction based on "antisymmetrical superexchange caused by spin-orbit coupling."

Let a general magnetic field $\vec{H}$ be applied at angles α_x, α_y, α_z, with respect to the x, y, and z axes of the crystal. The free energy in this magnetic field is minimized with respect to each vector component of $\vec{\lambda}$ and $\vec{\mu}$ resulting in the following six equations:

$$\partial\tilde{\Phi}/\partial\lambda_x = 2M_o(A\lambda_x + C\lambda^2\lambda_x + D\mu_y) = 0 \qquad (2a)$$

$$\partial\tilde{\Phi}/\partial\lambda_y = 2M_o(A\lambda_y + C\lambda^2\lambda_y - D\mu_x) = 0 \qquad (2b)$$

$$\partial\tilde{\Phi}/\partial\lambda_z = 2M_o(A\lambda_z + C\lambda^2\lambda_z + a\lambda_z) = 0 \qquad (2c)$$

$$\partial\tilde{\Phi}/\partial\mu_x = 2M_o(B\mu_x - D\lambda_y - H\cos\alpha_x) = 0 \qquad (2d)$$

$$\partial\tilde{\Phi}/\partial\mu_y = 2M_o(B\mu_y + D\lambda_x - H\cos\alpha_y) = 0 \qquad (2e)$$

$$\partial\tilde{\Phi}/\partial\mu_z = 2M_o(B\mu_z - H\cos\alpha_z) = 0 \qquad (2f)$$

Toru Moriya[23] published these equations for weak ferromagnetic materials in 1964.

The Dzialoshinskii-Moriya constant as written in Equation (1) is positive for otherwise the magnetic canting which causes the weak ferromagnetism would increase the free energy. From Equation (1) we see that if the anisotropic interaction 'a' is positive, then the free energy will be less for λ_z equal to zero than for other values. On the other hand, for a negative interaction 'a', the free energy is less for λ_x and λ_y equal to zero. Iron borate has a large positive anisotropic interaction[19] (for temperatures below the Curie temperature), and therefore, λ_z is zero, (to the order of terms given in the free energy). Hence Equation (2c) is identically zero.

In the absence of a magnetic field, μ_z is zero according to equation (2f). Therefore the spontaneous ferromagnetic moment of iron borate, if any, lies in the x-y plane (basal plane) of the crystal. Experimentally the magnetic anisotropy in the basal plane is less than one oersted.[4] For the experimental conditions used (minimum field of thirty-nine oersted), the magnetization in the basal plane will rotate until it is aligned with the component of $\vec{H}$ in the basal plane. Therefore, we now redefine the x axis to be parallel to this component of $\vec{H}$. The y axis is chosen to obtain a right-handed Cartesian coordinate system. Equations (2a) and (2e) are now identically zero. $H\cos\alpha_x$, $H\cos\alpha_y$, and $H\cos\alpha_z$ are denoted by H_x, H_y and H_z respectively. H_y is identically zero for our choice of coordinate axes. The general equations (2a) - (2f) are reduced to

$$A\lambda_y + C\lambda_y^3 - D\mu_x = 0 \tag{3a}$$

$$B\mu_x - D\lambda_y = H_x \tag{3b}$$

$$B\mu_z = H_z. \tag{3c}$$

At high temperatures the only long range order is that induced by the external field. Then the antiferromagnetic ordering (λ_y) is negligible. From equations (3b) and (3c) the magnetic susceptibility χ is found to be

$$\chi_x = m_x/H_x = 2M_o\mu_x/H_x$$
$$= 2M_o/B$$
$$\chi_z = m_z/H = 2M_o\mu_z/H_z$$
$$= 2M_o/B.$$

We see that χ is isotropic and proportional to 1/B. As the temperature drops, the susceptibility increases and B decreases. In canted antiferromagnets, B never becomes negative as it does in ferromagnets below the Curie temperature.

As the temperature is lowered we can no longer ignore antiferromagnetic ordering. Rearranging Equation (3b) to get μ_x and substituting it in Equation (3a) we obtain

$$C\lambda_y^3 + (A-D^2/B)\lambda_y = (D/B)H_x. \tag{4}$$

A.S. Borovik-Romanov and V.I. Ozhogin[14] derived this equation in 1960. In the limit as H goes to zero, we find

$$\lambda_y = [-(A-D^2/B)/C]^{\frac{1}{2}} \tag{5a}$$

$$\mu_x = (D/B)[-(A-D^2/B)/C]^{\frac{1}{2}}, \tag{5b}$$

or

$$\lambda_y = 0 \tag{5c}$$

$$\mu_x = 0. \tag{5d}$$

In the terminology of Landau[24] the state of a body in a second order phase transition changes continuously at the Curie temperature, but the symmetry undergoes a discontinuous change. This is possible because an arbitrarily small distortion in the geometry changes the symmetry. In this case, at T_C, we have the appearance of long range magnetic order. This ordering begins at zero and increases as the temperature is lowered. This aspect can be identified with solutions (5a) and (5b) below T_C if

$$A-D^2/B < 0 \tag{6a}$$

and

$$C > 0. \tag{6b}$$

These conditions give real positive values for λ_y and μ_x and a stable minimum in the free energy. Above T_c, only solutions (5c) and (5d) apply, denoting the absence of long range magnetic order. However, we must have

$$A-D^2/B > 0 \tag{6c}$$

and

$$C > 0 \tag{6d}$$

to insure a stable minimum in the free energy. In order for μ_x and λ_y to be continuous, at the Curie temperature we must have

$$A-D^2/B = 0. \tag{6e}$$

With an applied magnetic field the equations are more complex. Eliminating λ_y from equation (4) we get

$$H_x = (B^2/D^2)(A-D^2/B)(\mu_x-H_x/B) + (CB^4/D^4)(\mu_x-H_x/B)^3. \tag{7}$$

Equation (7), for non-zero H_x, has one and only one positive solution for $(\mu_x - H_x/B)$ at all temperatures by Descartes' rule of signs. Thus an external magnetic field with a component in the basal plane creates long range magnetic order at all temperatures and a Curie temperature is not defined by Landau's criterion. However, in a zero magnetic field, Landau's criterion for the Curie temperature can be used when other thermodynamic variables such as pressure vary.

To simplify the notation define

$$\xi_1 = (B^2/D^2)(A-D^2/B) \tag{8a}$$

$$\xi_2 = CB^4/D^4 \tag{8b}$$

$$\mu_x' = \mu_x - H_x/B \tag{8c}$$

$$\mu_z' = \mu_z - H_z/B \tag{8d}$$

$$\varepsilon = (T-T_C)/T_C^\circ. \tag{8e}$$

'ε' is a reduced temperature which is zero at T_C, and T_C° is the Curie temperature at one atmosphere of pressure.

In the new notation the Equations (3c) and (7) become

$$H_x = \xi_1 \mu_x' + \xi_2 (\mu_x')^3 \tag{9a}$$

$$0 = \mu_z'. \tag{9b}$$

In analytical form these equations are similar to those decribing the second order phase transitions in ferromagnets, (see K.P. Belov[25]). Of course here only the component of the magnetic field in the basal plane is effective. The form of equation (9a) suggests the technique of plotting H_x/μ_x' versus $(\mu_x')^2$ to determine T_C (at which ξ_1 is zero) provided B has been estimated beforehand. This technique is standard in ferromagnetism.

Following Landau's[26] ideas, Borovik-Romanov[14] and Toru Moriya[23] assumed the following functional temperature dependences

$$\xi_1 = (B^2/D^2)\nu''\varepsilon \tag{10a}$$

and

$$\xi_2 = CB^4/D^4 \tag{10b}$$

where ν'' is a positive constant. These dependences are the simplest ones which satisfy equations (6a) - (6e). The relationships given by equation (10a) and (10b) will be called the linear assumption. Substituting in Equation (5b) we find

$$\mu_x' = (-\xi_1/\xi_2)^{\frac{1}{2}}$$

$$= (D/B)[\nu''(T_c-T)/CT_c^\circ]^{\frac{1}{2}} \tag{10c}$$

This is the result for the classical Landau Theory. However, experiments do not show a $(T_c-T)^{\frac{1}{2}}$ temperature dependence for the spontaneous magnetization in most substances.

Critical Exponents of Single Crystals

The theory of 'static scaling' in a critical region provides another choice to satisfy Equations (6a) - (6e). Using static scaling Robert Brout[27] gives the following equation of state above the Curie temperature

$$\varepsilon^{\gamma} m f(m^2/\varepsilon^{2\beta}) - H = 0 \tag{11a}$$

where

$f(m^2/\varepsilon^{2\beta})$ = some function of the variable $m^2/\varepsilon^{2\beta}$,

m = the magnetization, and

γ, β = critical exponents.

Approximating $f(m^2/\varepsilon^{2\beta})$ by a power series, we have

$$f(m^2/\varepsilon^{2\beta}) \simeq k_1 + k_2 m^2/\varepsilon^{2\beta}$$

where k_1 and k_2 are constants. The power series approximation is accurate near T_C only in limit of zero magnetic field. This insures that m will be small as ε approaches zero at T_C. Equation (11a) with this substitution becomes

$$H \simeq k_1 \varepsilon^{\gamma} m + k_2 \varepsilon^{\gamma-2\beta} m^3 \tag{11b}$$

Comparing this equation with equation (9a) suggests that above T_C one should choose

$$\xi_1 = (B^2/D^2)\nu\varepsilon^{\gamma} \tag{12a}$$

and

$$\xi_2 = (C_o B^4/D^4)\varepsilon^{\gamma-2\beta} \tag{12b}$$

where C from equation (1) has been written as

$$C = C_o \varepsilon^{\gamma-2\beta}.$$

If this formulation can be extended below the Curie temperature[27] one must use the absolute value of ε. It is, of course, possible that equation (11a) has a different temperature dependence below T_C and that β, γ, ν, and C also have different values. Consequently, we can have

$$\xi_1 = -(B^2/D^2)\nu'|\varepsilon|^{\gamma'} \tag{12c}$$

and

$$\xi_2 = (C_0'B^4/D^4)\,|\epsilon|^{\gamma'-2\beta'} \qquad (12d)$$

Primed constants are used below T_c and unprimed above. With the expressions for ξ_1 and ξ_2 from static scaling theory, Equation (5b) becomes

$$\mu_x = (D/B)\,(\nu'/C_0')^{\frac{1}{2}}\,|\epsilon|^{\beta'}$$

The temperature dependence for spontaneous magnetization is $(T_c-T)^{\beta'}$ instead of $(T_c-T)^{\frac{1}{2}}$. For many magnetic materials the experimental value of β' is near 1/3. The relationships in Equation (12a) - (12d) will be called the rational exponent assumption. Note that the two assumptions coincide if $\gamma = \gamma' = 1$ and $\beta = \beta' = \frac{1}{2}$. The theory will be developed using the more general rational exponent assumption. If the corresponding relationships based on the linear assumption are desired, then the appropriate values of γ, γ', β, and β' can be inserted. In the absence of a magnetic field the above choices for ξ_1 and ξ_2 are consistent with the group theory and experimental data. However, at T_c the above formulation is inadequate since Equation (11b) predicts an infinite magnetization in the presence of a magnetic field. The limiting form for $f(m^2/\epsilon^{2\beta})$ at T_c for non-zero H can be found using Equation (11a). In order to cancel the ϵ singularity at T_c it is necessary that

$$\lim_{\epsilon\to 0^+} f(m^2/\epsilon^{2\beta}) = k_3\,(m^2/\epsilon^{2\beta})^{\gamma/2\beta}$$

and

$$\lim_{\varepsilon \to 0^-} f(m^2/|\varepsilon|^{2\beta'}) = k_3'(m^2/|\varepsilon|^{2\beta'})^{\gamma'/2\beta'}$$

where k_3 and k_3' are constants. Then at T_c we have

$$k_3 m^{1+\gamma/\beta} - H = 0$$

and

$$k_3' m^{1+\gamma'/\beta'} - H = 0.$$

Uniqueness of the magnetization at T_c requires that $\gamma/\beta = \gamma'/\beta'$ and $k_3 = k_3'$. At T_c we have

$$m^{\delta} = (H/k_3) \tag{13}$$

where

$$\delta = 1 + \gamma/\beta.$$
$$= 1 + \gamma'/\beta'$$

Scaling theory gives two limiting forms for the magnetization near T_c. In the limit as $H \to 0$ Equation (11b) can be used except at T_c. For non-zero H Equation (13) will be assumed to dominate very near T_c and be correct at T_c.

In order to obtain simple expressions, the solution for the magnetization in a non-zero magnetic field is derived for each of three temperature regimes; $T < T_c$, $T = T_c$, and $T > T_c$. For temperatures below the Curie temperature, we follow the inversion method of Borovik-Romanov and Ozhogin[14]. That is, the $H_x = 0$

solution is used as a zero order term for the magnetization and we calculate the correction $\tau(H_x)$ caused by a small magnetic field. Adding this correction to Equation (10c) we have

$$\mu_x' = (-\xi_1/\xi_2)^{\frac{1}{2}} + \tau$$

Substituting in Equation (9a) we get

$$H_x = \xi_1[(-\xi_1/\xi_2)^{\frac{1}{2}} + \tau] + \xi_2[(-\xi_1/\xi_2)^{\frac{1}{2}} + \tau]^3.$$

Keeping terms only to the first order in τ we obtain

$$\tau = -H_x/2\xi_1.$$

Then

$$\mu_x \simeq (-\xi_1/\xi_2)^{\frac{1}{2}} - (1/2\xi_1 - 1/B) \qquad (14)$$

Using the rational exponent assumption to predict the temperature dependence of ξ_1 and ξ_2, we obtain a spontaneous magnetic moment $(m_x)_s$ of

$$(m_x)_s = 2M_o(D/B)(\nu'/C_o')^{\frac{1}{2}}[(T_c-T)/T_c^o]^{\beta'} \qquad (15a)$$

Below T_c the magnetic differential susceptibility χ_x is defined by

$$\chi_x = [m_x - (m_x)_s]/H_x.$$

In the limit as H_x becomes zero we get

$$\chi_x = 2M_o(1/B - 1/2\xi_1)$$

$$= (2M_o/B)\{1 + (D^2/2\nu'B)[T_c^o/(T_c-T)]^{\gamma'}\}. \qquad (15b)$$

For temperatures above T_c the spontaneous magnetization is zero. Using Newton's[28] method to invert Equation (9a) we find

$$\mu_x \simeq (1/\xi_1 + 1/B)H_x - (\xi_2/\xi_1^4)H_x^3. \qquad (16)$$

As H_x goes to zero we obtain for the magnetic susceptibility χ_x

$$\chi_x = (2M_o/B)\{1 + (D^2/\nu B)[T_c^o/(T-T_c)]^\gamma\}. \qquad (17)$$

From the coefficient of H_x^3 in Equation (16) we can find a relation for β above T_c, that is,

$$\xi_2/\xi_1^4 = (C_o D^4/\nu^4 B^4)\varepsilon^{-3\gamma-2\beta}$$

Toru Moriya[23] derived equations similar to Equations (15a), (15b), and (17) in 1964 but he used the linear assumption. That is, his equations use ½ instead of β' and 1 in place of γ and γ'.

The last temperature region to be considered is that near T_c. Exactly at T_c, Dzialoshinskii's theory using the linear assumption gives

$$[m_x/2M_o - H_x/B]^3 = (D^4/CB^4)H_x \qquad (18)$$

because ξ_1 is zero. From scaling theory the magnetization at T_c should be of the form of Equation (13) where δ is not necessarily 3. Experiments have found δ ranging from 3 to 6. Substituting δ for 3 and the arbitrary constant $(2M_o)^\delta k_3$ for ξ_2 in Equation (9a) to impose agreement with scaling theory at T_c and using $\xi_1\mu_x'$ as a small correction term, we obtain

$$m_x = (H_x/k_3)^{1/\delta} - (\xi_1/2M_o\delta H_x)(H_x/k_3)^{2/\delta} + 2M_o H_x/B \qquad (19)$$

Critical Exponents for a Powdered Sample

We now examine the modifications necessary to relate the magnetic properties of a powder to a single crystal of $FeBO_3$. As discussed previously, iron borate has a basal plane of easy magnetization. Hence, magnetization in the basal plane will be aligned with the component of $\vec{H}$ in that plane. Figure 16 defines the coordinates for a general crystallite in a magnetic field.

The component of magnetization along the magnetic field m_H is

$$m_H = m \cos (90-\theta-\phi)$$

$$= m_x \sin\theta + m_z \cos\theta.$$

Inverting Equation (7) we obtain

$$\mu_x = H_x/B + g(H_x)$$

where g is the appropriate inverse function. Using this expression and Equation (3c), we obtain for m_H

$$m_H = 2M_oH/B + 2M_og(H\sin\theta)\ \sin\theta$$

Note that the first term on the right is independent of the alignment of the crystallite and, thus, it is the same for a powdered sample or a single crystal.

We now assume that the crystallite orientations have a probability distribution $P(\theta)$. The crystallite orientations are considered to be randomly distributed with respect to rotations about $\vec{H}$ and therefore, the probability distribution only needs to specify θ. A possible non-random distribution for $P(\theta)$ can

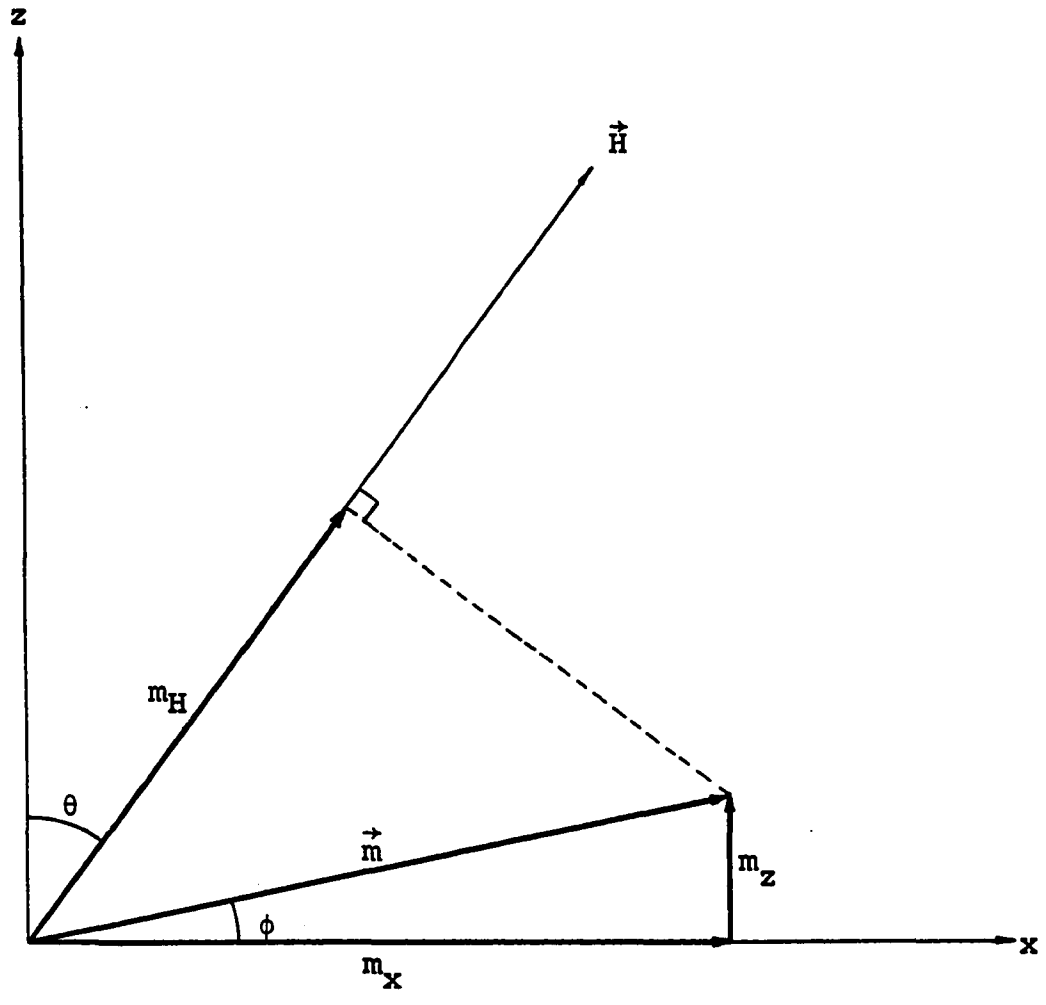

Figure 16. Coordinate System for a Randomly Oriented Crystallite in a Magnetic Field. The z axis is perpendicular to the basal plane of the crystallite. The x axis is chosen to lie in the z-$\vec{H}$ plane. Because of the low anisotropy field in the basal plane, the magnetization rotates until it has no component perpendicular to the z-$\vec{H}$ plane.

arise from partial alignment of the crystallites during the initial application of the magnetic field. The average magnetization $\langle m_H \rangle$ is parallel to $\vec{H}$ and is given by

$$\langle m_H \rangle = (2M_o H/B) + 2M_o \int_0^{\pi} P(\theta)\, g(H\sin\theta)\, \sin\theta\, d\theta \qquad (20)$$

where

$$\int_0^{\pi} P(\theta)\, d\theta = 1.$$

We define

$$s_n = \int_0^{\pi} P(\theta)\, \sin^n\theta\, d\theta.$$

For a randomly oriented sample $P(\theta)$ is $\frac{1}{2}\sin\theta$; thus, s_1 and s_2 are $\pi/4$ and $2/3$ respectively. For fully aligned crystals all s_n are 1.

Below T_c, using Equations (14) and (20), we find a spontaneous magnetization of

$$\langle m_H \rangle_s = (2M_o s_1 D/B)(\nu'/C_o')^{\frac{1}{2}}[(T_c - T)/T_c^o]^{\beta'} \qquad (21a)$$

and an initial differential susceptibility of

$$\langle \chi_H \rangle = (2M_o/B)\{1 + (s_2 D^2/2\nu' B)[T_c^o/(T_c - T)]^{\gamma'}\} \qquad (21b)$$

Above T_c, but now using Equation (16), we obtain for the initial susceptibility

$$\langle \chi_H \rangle = (2M_o/B)\{1 + (s_2 D^2/\nu B)[T_c^o/(T - T_c)]^{\gamma}\}. \qquad (22)$$

Near T_c the magnetization, based on Equation (19), is

$$\langle m_H \rangle = (H/k_3)^{1/\delta} s_{(1+1/\delta)} - (\xi_1/2M_o\delta H)(H/k_3)^{2/\delta} s_{2/\delta} + 2M_oH/B. \quad (23)$$

Comparing powder and single crystal magnetic properties, we find the same exponents but differing coefficients. Therefore, the critical exponents of $FeBO_3$ can be determined from a powdered sample.

Entropy and Specific Heat

For a consistent thermodynamic theory, the magnetic transition at the Curie temperature must be of second order. In the limit of zero magnetic field the rational exponent assumption gives a second order transition as will be shown by the behavior of the entropy and specific heat at T_c.

In a zero magnetic field the free energy of a powdered sample is identical to that of a single crystal of the same weight if we neglect the effects of particle interactions, domains, etc. The magnetic part of Dzialoshinskii's free energy Φ_m for a single crystal (or a powder sample) at H = 0 is

$$\Phi_m = \Phi - \Phi_o$$

$$= 2M_o[\tfrac{1}{2} A\lambda^2 + \tfrac{1}{2}B\mu^2 + \tfrac{1}{4}C\lambda^4 - D\lambda_y\mu_x].$$

The entropy of the magnetic part of this free energy S_m is found from

$$S_m = -(\partial\Phi_m/\partial T)_p$$

$$= -(1/T_c^o)(\partial\Phi_m/\partial\varepsilon)_p.$$

Using the rational exponent assumption, we have

$$\Phi_m = 2M_o[-(B^2\nu'/2D^2)|\varepsilon|^{\gamma'}(\mu_x)_s^2 + (C_o'B^4/4D^4)|\varepsilon|^{\gamma'-2\beta'}(\mu_x)_s^4]$$

below T_c and a similar equation without primes above T_c. But above T_c $(\mu_x)_s$, Φ_m, and S_m are identically zero.

Below T_c we get

$$S_m = -2M_o[(\nu')^2(\gamma'+2\beta')/4C_o'T_c^o]|\varepsilon|^{\gamma'+2\beta'-1}$$

since

$$\partial\Phi_m/\partial(\mu_x)_s = 0$$

and

$$(\mu_x)_s^2 = (D^2\nu'/B^2C_o')|\varepsilon|^{2\beta'}.$$

The magnetic part of the specific heat $(C_p)_m$ is determined from

$$(C_p)_m = T(\partial S_m/\partial T)_p$$

$$= (T/T_c^o)(\partial S_m/\partial\varepsilon)_p.$$

Below T_c we have

$$(C_p)_m = 2M_o(\nu'/T_c^o)^2(\gamma'+2\beta')(\gamma'+2\beta'-1)(T/4C_o')|\varepsilon|^{\gamma'+2\beta'-2}$$

and above T_c, $(C_p)_m$ is zero.

The specific heat and entropy reduce to Landau's[24] expressions when γ' is 1 and β' is ½. Experimentally the value of $\gamma' + 2\beta'$ lies between one and two. For these materials (including $FeBO_3$), the entropy is continous and the specific heat, discontinuous at T_c. Thus the transition is of second order.

Pressure Effect

Hydrostatic pressure can affect the magnetization and the Curie temperature of a ferromagnetic sample.[29] The energy due to the exchange (or superexchange) interaction depends on the distance between the atoms in a crystal. K.P. Belov[25] discusses this effect in ferromagnets for a linear change in the exchange energy with pressure. Here a slightly different approach will be adopted. For pressures of a few kilobar, only a relatively small change in the interatomic spacing occurs. A linear change in J, the exchange parameter, and thus a linear shift in the Curie temperature with pressure will be assumed. That is,

$$\Delta T_c(p) = T_c(p) - T_c^\circ$$

$$= \zeta p$$

where ζ is the proportionality constant. To a first order we have

$$\vec{m}(p,T,\vec{H}) = \vec{m}([T - T_c(p)],\vec{H})$$

$$= \vec{m}(\{[T - \Delta T_c(p)] - T_c^\circ\},\vec{H}). \qquad (24)$$

The shift in magnetization caused by pressure is equivalent to a change in the temperature.

A relationship between pressure and magnetization is obtained from the approximation

$$\Delta\langle m_H\rangle_s \simeq \frac{\partial\langle m_H\rangle_s}{\partial[T_c(p)-T]} \frac{\partial[T_c(p)-T]}{\partial p}\Delta p.$$

Using this approximation with Equation (21a), we find

$$\Delta\langle m_H\rangle_s \simeq \{\beta'\zeta p/[T_c(p) - T]\}\langle m_H\rangle_s.$$

Following the above procedure with Equation (21b), we have for the change in the initial differential susceptibility below T_c

$$\Delta\langle\chi_H\rangle \simeq - \{\gamma'\zeta p/[T_c(p) - T)\}(\langle\chi_m\rangle - 2M_o/B).$$

Above T_c using Equation (22) we obtain

$$\Delta\langle\chi_H\rangle \simeq \{\gamma\zeta p/[T - T_c(p)]\}(\langle\chi_H\rangle - 2M_o/B).$$

These equations, because of the $T_c(p) - T$ factor in their denominator, predict that pressure will have a maximum relative effect near T_c. The data will indicate how well a linear shift in the Curie temperature describes the effect of pressure on $FeBO_3$.

CHAPTER VI

ANALYSIS AND RESULTS

Critical Exponents

The critical exponents are determined from the temperature dependence of the spontaneous magnetization and initial susceptibility, and from the magnetic field dependence of the magnetization at T_c. The magnetization at various temperatures as a function of magnetic field is shown in Figure 17. Analysis of the data to determine the critical exponents is separated into the three temperature regions, $T < T_c$, $T \simeq T_c$, and $T > T_c$.

Before the spontaneous magnetization and initial differential susceptibility below T_c can be found, the effects of domains, strain, etc., must be taken into account. These effects become less important as the magnetic field increases. This behavior, which is empirically described by an exponentially decreasing term, is included as a correction to the measured magnetization. That is, the data is fit to

$$\langle m_H \rangle = a_1(T) + b_1(T)H - c_1\exp(-d_1H).$$

The spontaneous magnetization is given by $a_1(T)$ and the initial differential susceptibility by $b_1(T)$.

Theoretically as T_c is approached, the approximation that

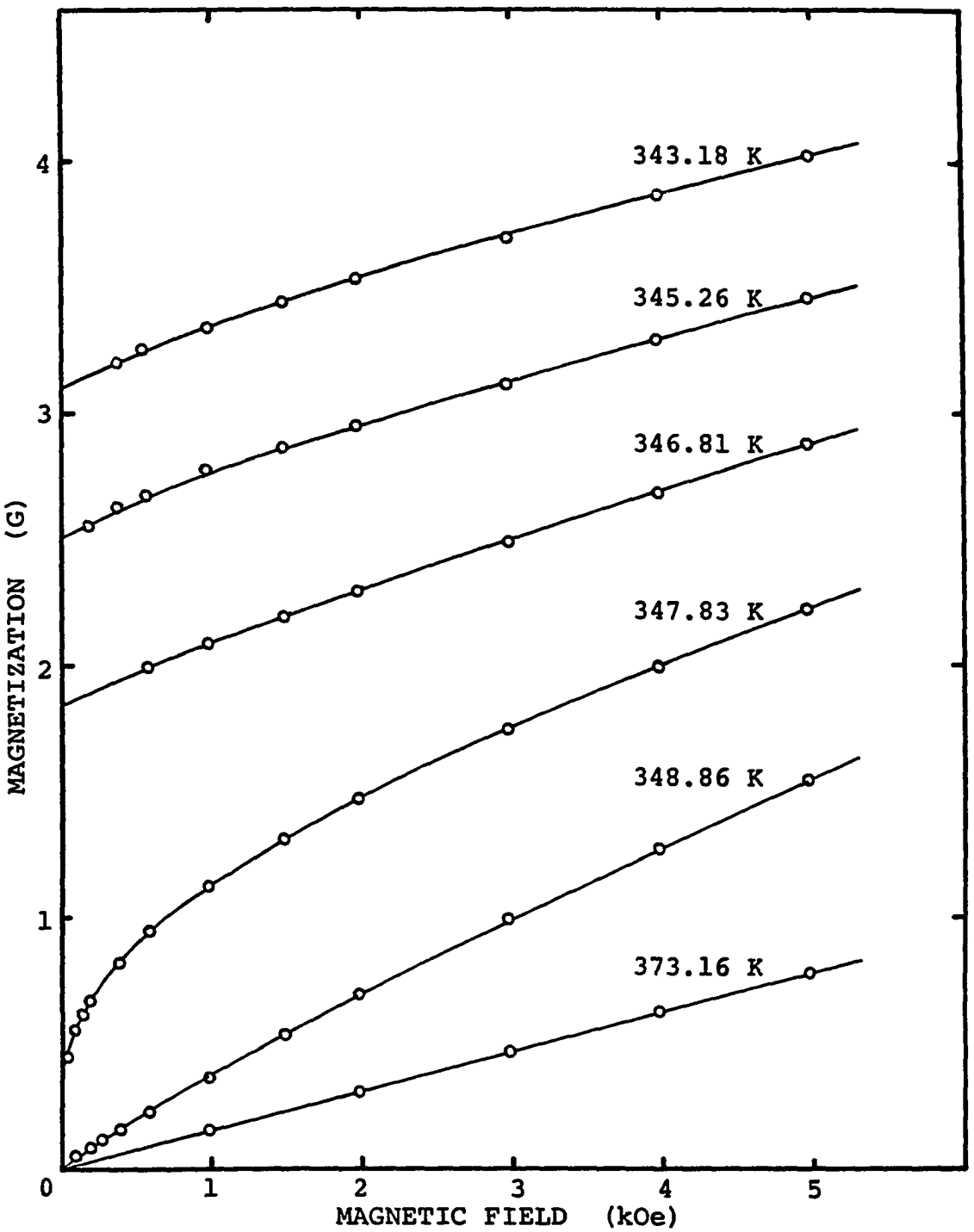

Figure 17. Magnetization as a Function of Temperature and Magnetic Field.

magnetization is a linear function of the magnetic field is good only for progressively smaller values of H. Experimentally the breakdown of the linear approximation for $H \leq 5$ kOe becomes evident when the temperature is within three degrees of T_c.

The values of c_1 and d_1 are determined by curve fitting data that is more than three degrees below T_c. Their values are 0.06 $\langle m_H \rangle$ and 2.3 kOe^{-1} respectively. Using these values for c_1 and d_1, we can adjust the magnetization when the temperature is within three degrees of T_c. After this adjustment, a linear dependence on H is recovered and the spontaneous magnetization and initial susceptibility can be obtained. Table II shows the values obtained.

Table II. Spontaneous Magnetization and Initial Susceptibility Below T_c

Temperature (K)	Saturation Magnetization, $a_1(T)$, (G)	Initial Susceptibility, $b_1(T)$, (G/kOe)
293.27	7.450	0.167
312.71	6.432	0.165
313.25	6.393	0.166
333.22	4.758	0.164
343.18	3.206	0.165
343.22	3.200	0.165
345.02	2.672	0.174
345.26	2.606	0.174
346.81	1.899	0.200
347.10	1.684	0.214
347.23	1.573	0.238
347.41	1.399	0.268
347.83	0.447	

Single crystal values for $4\pi m_s$ at 297-300 K are reported by A. J. Kurtzig[3] and M. P. Petrov[7] to be 115 G and 122 G respectively. A randomly oriented powder will have a value of $\pi/4$ times less or 90 to 96 G. The $4\pi\langle m_H\rangle_s$ value for our sample is 91 G. This indicates that the powder has little, if any, alignment.

At the Curie temperature the spontaneous magnetization becomes zero. From Equation (21a), $\langle m_H\rangle_s^{1/\beta'}$ approaches T_c linearly. Using this and an initial value[8] for β' in Figure 18, we find T_c to be 347.85 K with a precision of ±0.03 K and an accuracy of ±0.2 K. The ratio B/D in Equation (21a) is independent of temperature according to M. P. Petrov.[7] Thus, the log-log plot of Equation (21a) in Figure 19 gives 0.350 ± 0.007 for β'.

The magnetic susceptibility in Equations (21b) and (22) approaches $2M_o/B$ far from T_c. The limiting values for $2M_o/B$ are 0.166 and 0.150 G/kOe at 293 K and 373 K respectively. Values at intermediate temperatures are obtained by linear interpolation. From the log-log plot of Equation (21b) (see Figure 20), we find that γ' is 1.0 ± 0.1.

Above T_c the magnetization has the functional dependence of Equation (16), that is

$$\langle m_H\rangle = a_2(T)H - b_2(T)H^3.$$

Using the initial susceptibility, $a_2(T)$, with Equation (22), we can find γ. Experimental values for $a_2(T)$ are shown in Table III.

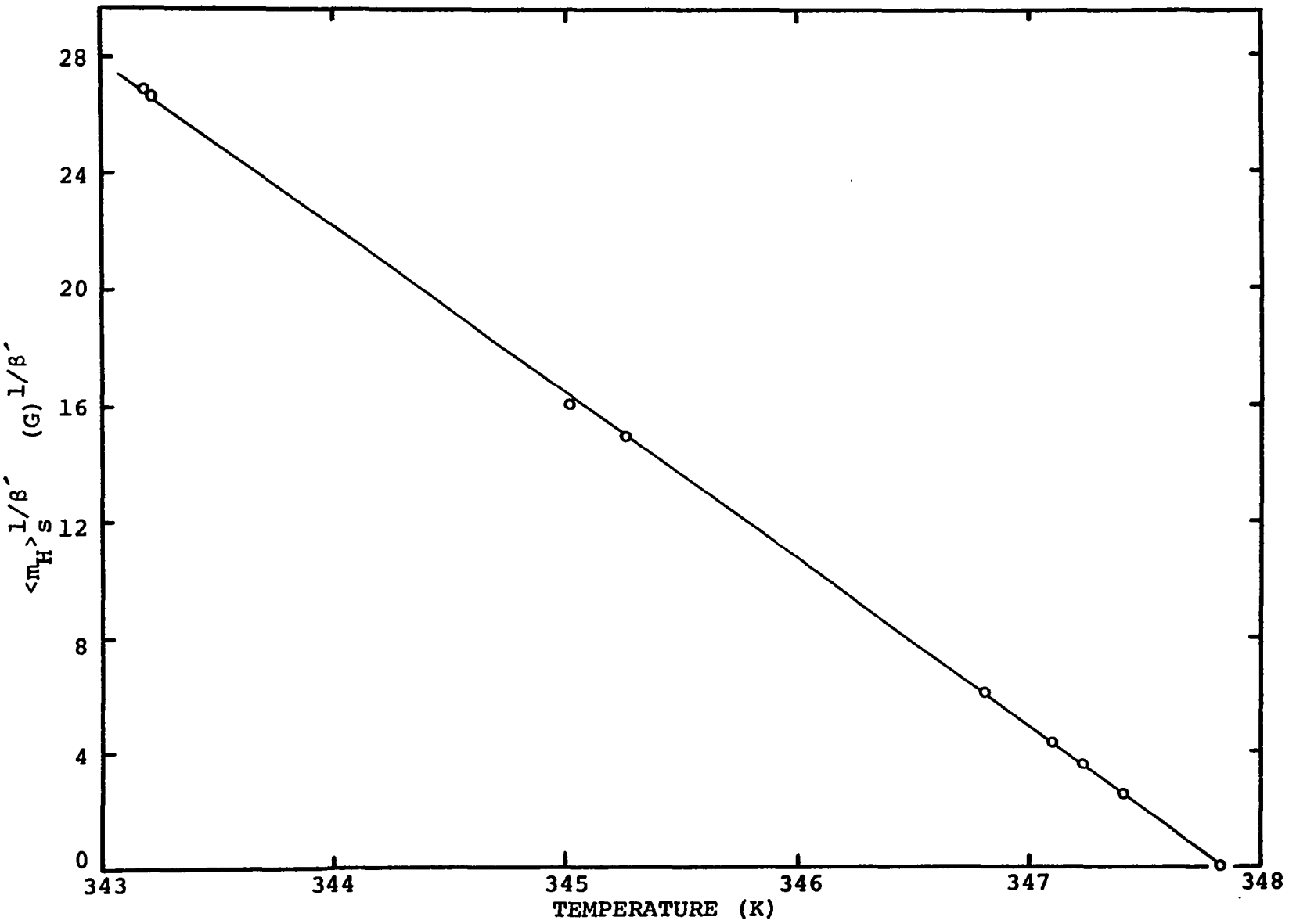

Figure 18. Extrapolation of the Spontaneous Magnetization to Find the Curie Temperature.

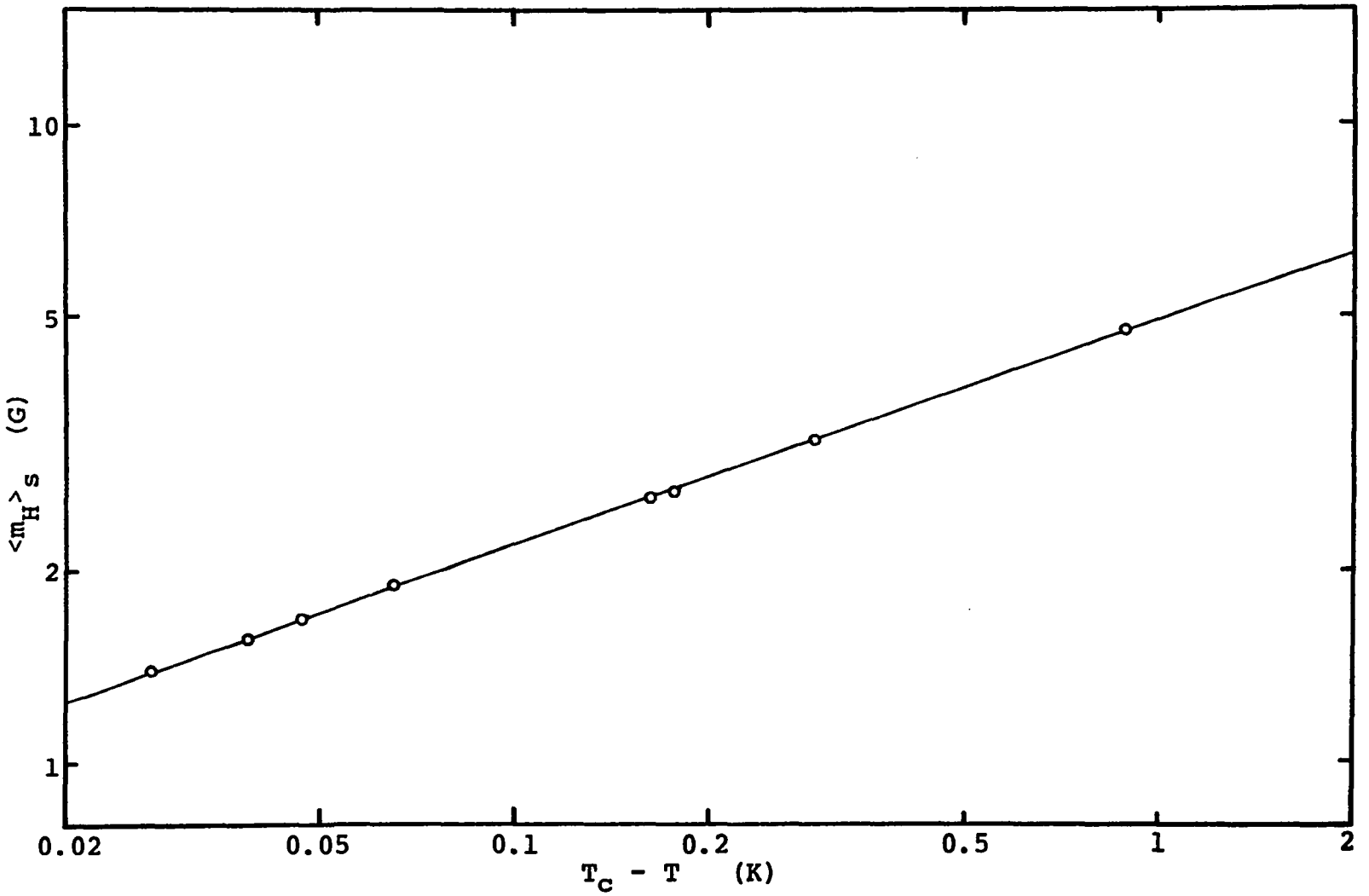

Figure 19. Log-Log Plot for Determining the Critical Exponent β'.

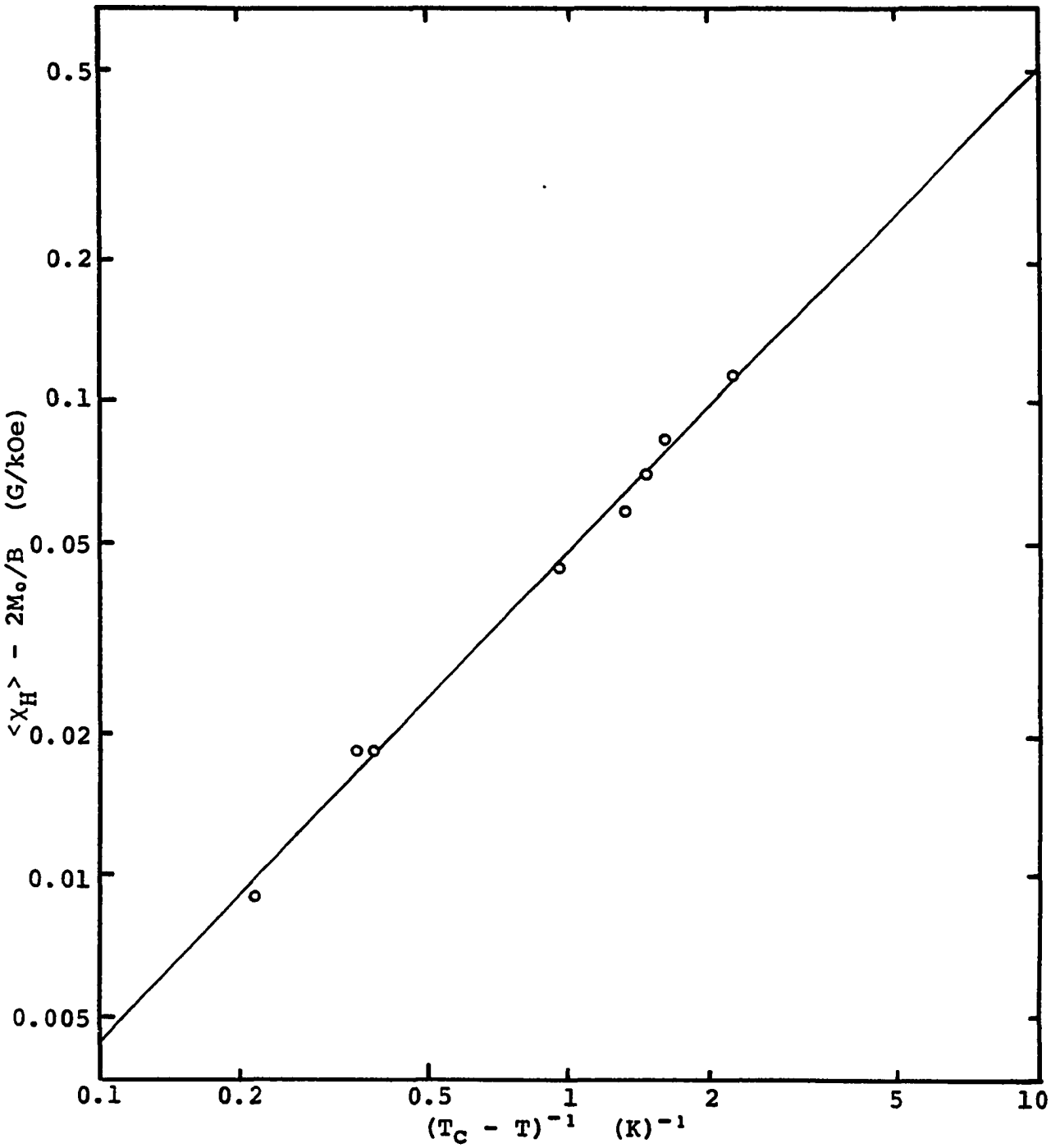

Figure 20. Log-Log Plot for Determining the Critical Exponent γ'.

Table III. Initial Susceptibility Above T_c

Temperature (K)	Initial Susceptibility, $a_2(T)$, (G/kOe)
348.46	0.58
348.86	0.373
349.21	0.284
350.16	0.2237
351.16	0.1948
353.16	0.1753
355.16	0.1660
363.16	0.1583
373.16	0.1552

Using the same log-log plotting technique as for γ' we find (see Figure 21) that γ is 1.38 ± 0.08.

Table IV gives the magnetization at various magnetic fields for three temperatures near T_c. At T_c, $\langle m_H \rangle - 2M_oH/B$ is proportional to $H^{1/\delta}$ according to Equation (23). A log-log plot using the above variables yields a line with a slope of $1/\delta$ at T_c. We find from Figure 22 that δ is 3.9 ± 0.4.

Equation (23) contains a correction term when the temperature differs from T_c. This term changes sign at T_c and also becomes smaller as H increases. Thus, Figure 22 should contain lines which approach an asymptotic slope of $1/\delta$ from different directions depending on whether the temperature is above or below T_c.

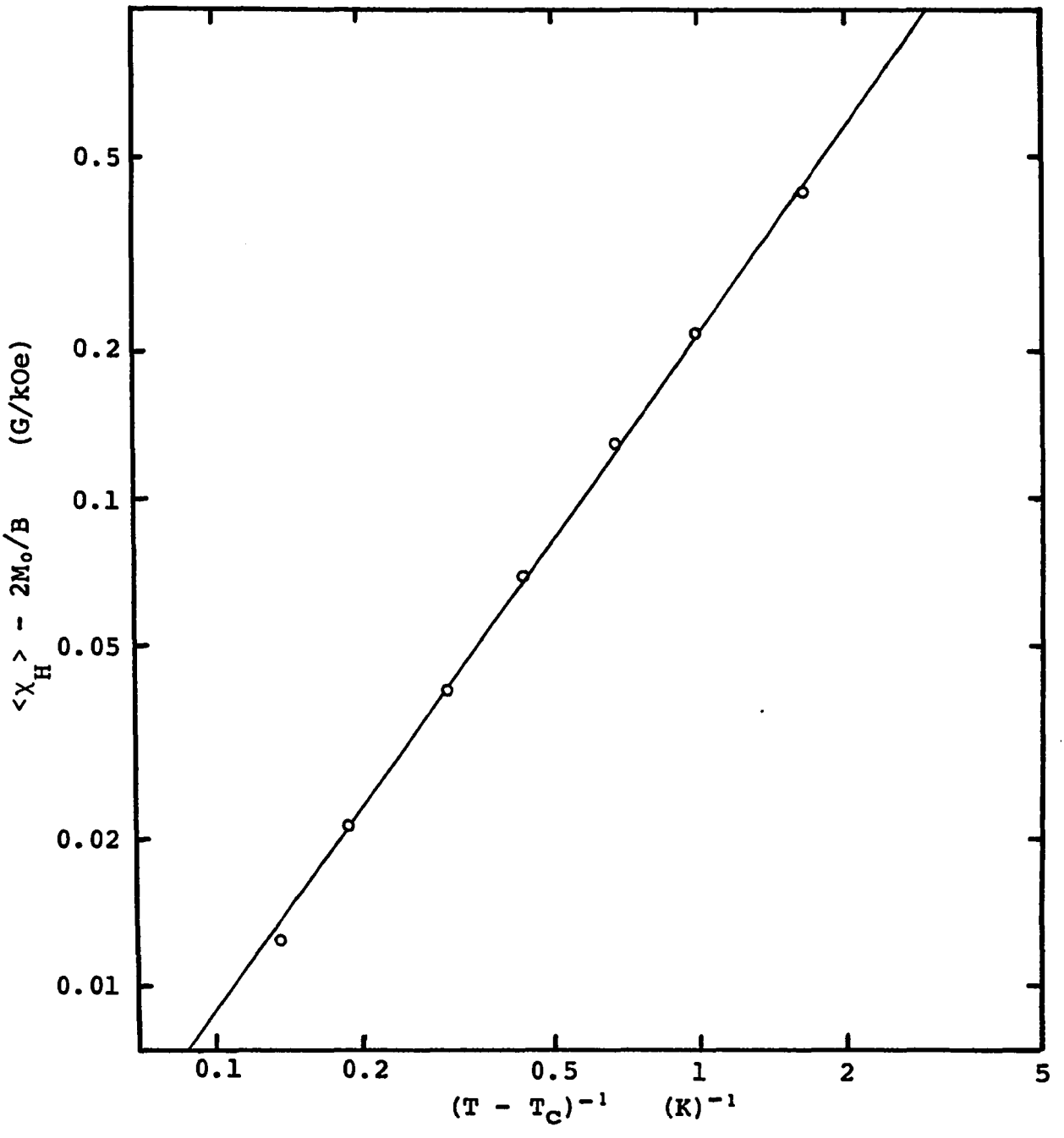

Figure 21. Log-Log Plot for Determining the Critical Exponent γ.

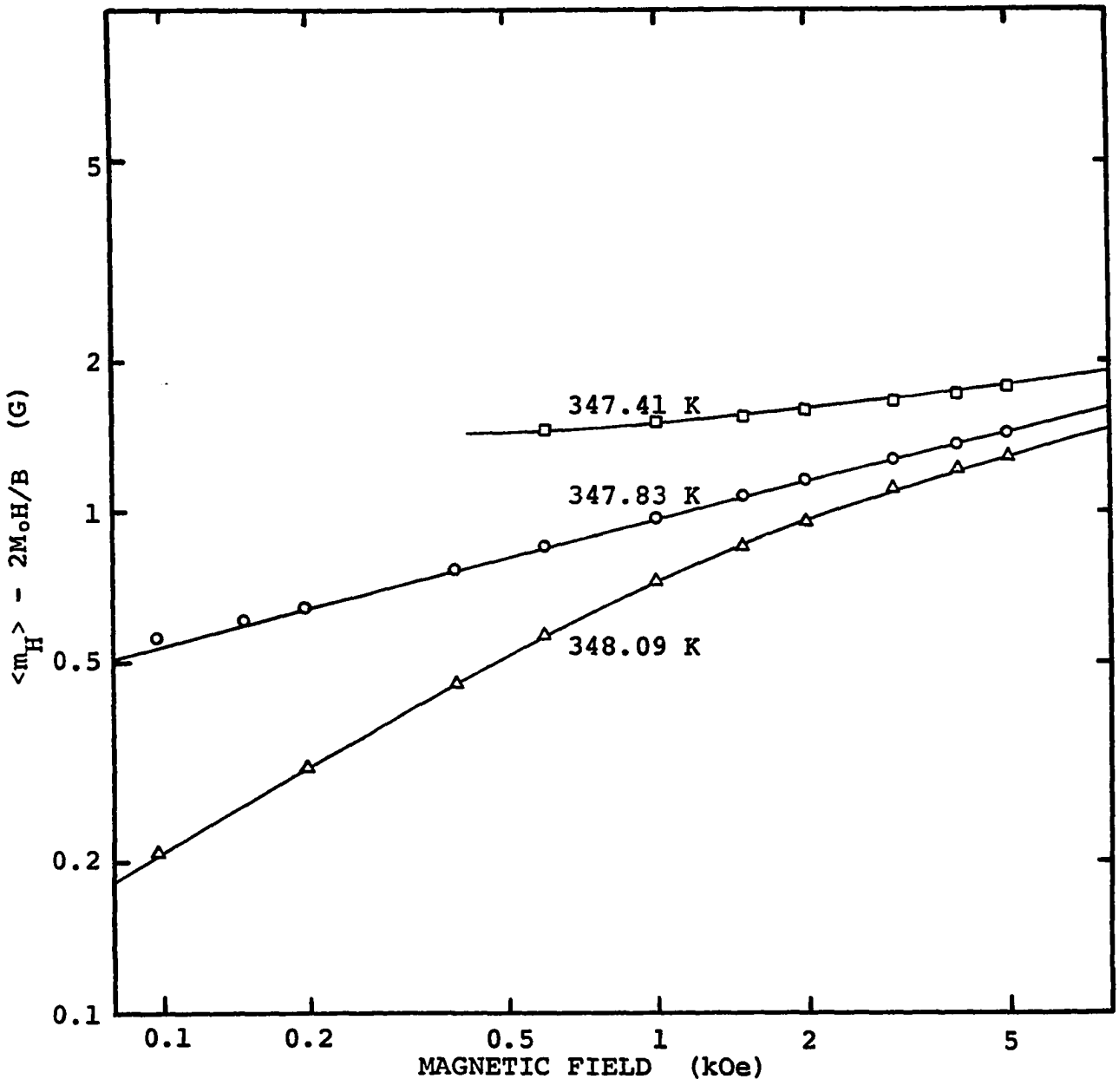

Figure 22. Log-Log Plot for Determining the Critical Exponent δ. The slope of the lines below and above 347.83 K approaches $1/\delta$ from different directions as the magnetic field increases.

Table IV. Magnetization as a Function of H for $T \simeq T_c$

Magnetic Field (kOe)	Magnetization (G) at Temperatures		
	347.41 K	347.83 K	348.09 K
.098		.5768	.2089
.148		.6319	
.198		.6849	.3350
.397		.8320	.5165
.596	1.5560	.9523	.6602
.995	1.6617	1.1274	.8780
1.494	1.7862	1.3124	1.0879
1.993	1.9043	1.4704	1.2651
2.992	2.1261	1.7441	1.5769
3.991	2.3389	1.9887	1.8308
4.989	2.5406	2.2199	2.0542

If this behavior, which is evident in Figure 22, is general, then this can be a criterion for determining T_c.

The results for the critical exponents of this work along with published values are shown in Table V. The values of β' agree. Those for δ disagree. This disagreement can be due to different methods of analysis or different definitions for the Curie temperature. The values for the Curie temperature differ slightly. If the Curie temperature of this dissertation had been determined from spontaneous magnetizations obtained solely by linear extrapolation from a high magnetic field or from the maximum, differential susceptibility in a high field, it would have been 0.5 K higher. The values of T_c could also differ because of variations in sample purity.

Table V. T_c and Critical Exponents for $FeBO_3$

T_c, Critical Exponent	Temperature Range for Determination	Source
T_c = 347.85 ± 0.2 K	333 - 348 K	
T_c = 348.35 ± 0.2 K	303 - 348 K	Ref. (8)
T_c = 348.5 ± 0.1 K		Ref. (9)
T_c = 348.2 ± 0.1 K		Ref. (30)
γ = 1.38 ± 0.08	$1.002 < T/T_c < 1.02$	
γ' = 1.01 ± 0.10	$0.985 < T/T_c < 0.999$	
β' = 0.350 ± 0.007	$0.95 < T/T_c < 0.9998$	
β'' = 0.354 ± 0.005	$0.940 < T/T_c < 0.9996$	Ref. (8)
β' = 0.353	$0.95 < T/T_c$	Ref. (9)
δ = 3.9 ± 0.4	$\lvert T - T_c \rvert < 0.03$ K	
δ = 3		Ref. (9)

Pressure Effect

The theory developed in Chapter V predicts that a change in magnetization caused by pressure is equivalent to a change in magnetization caused by an appropriate shift in temperature. Figure 23 shows that the magnetization as a function of temperature does follow a similar pattern at two different pressures. Therefore, the critical exponents are not sensitive functions of pressure and the theory applies.

The effect of pressure on the spontaneous magnetization is analyzed first. The data is shown in Table VI.

Table VI. Spontaneous Magnetization as a Function of Pressure

Temperature (K)	Spontaneous Magnetization (G) at Pressures		
	1 kbar	2 kbar	3 kbar
313.25	6.418	6.450	6.487
333.22	4.814	4.876	4.932
343.22	3.340	3.463	3.568
345.26	2.798	2.953	3.123
347.23	1.963	2.263	2.501
348.34	0.481	1.521	1.926
349.34			0.948

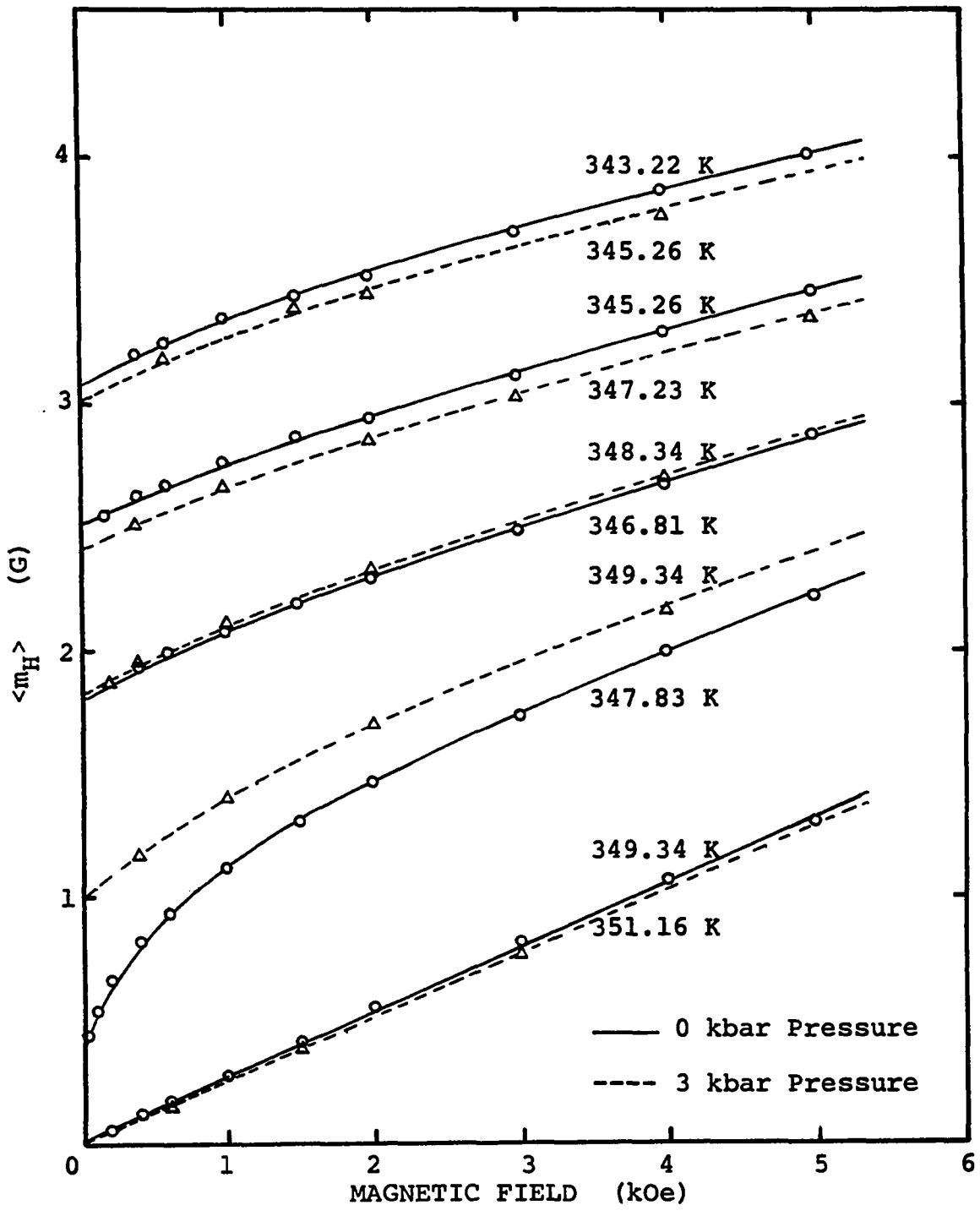

Figure 23. Magnetization as a Function of Magnetic Field at 0 and 3 kbar Pressure.

Figure 24 shows $\langle m_H \rangle_s^{1/\beta'}$ as a function of temperature at the four pressures. The data can be fit to parallel straight lines indicating that β' is not a function of pressure within experimental error. The intercepts are the Curie temperatures at the given pressure. These intercepts and the change in T_c with pressure are shown in Table VII.

Table VII. Curie Temperature as a Function of Pressure Determined from the Spontaneous Magnetization

$T_c(p)$ (K)	Pressure (kbar)	$T_c(p) - T_c(0)$ (K)
347.85 ± 0.03	0	
348.37 ± 0.03	1.00 ± 0.02	0.52
348.88 ± 0.04	2.00 ± 0.02	1.03
349.40 ± 0.06	3.00 ± 0.02	1.55

The change of T_c with pressure is linear. The error in the Curie temperatures is obtained from the scatter of the data about the line.

Figure 25 is similar to Figure 24 but it has a temperature scale chosen to include all of the pressure versus spontaneous magnetization data. The parallelism of the curves shows that, within experimental error, the shift in T_c accounts for all of the change in the magnetization. The lines in Figure 25 are no longer straight below 320 K indicating that scaling theory is breaking

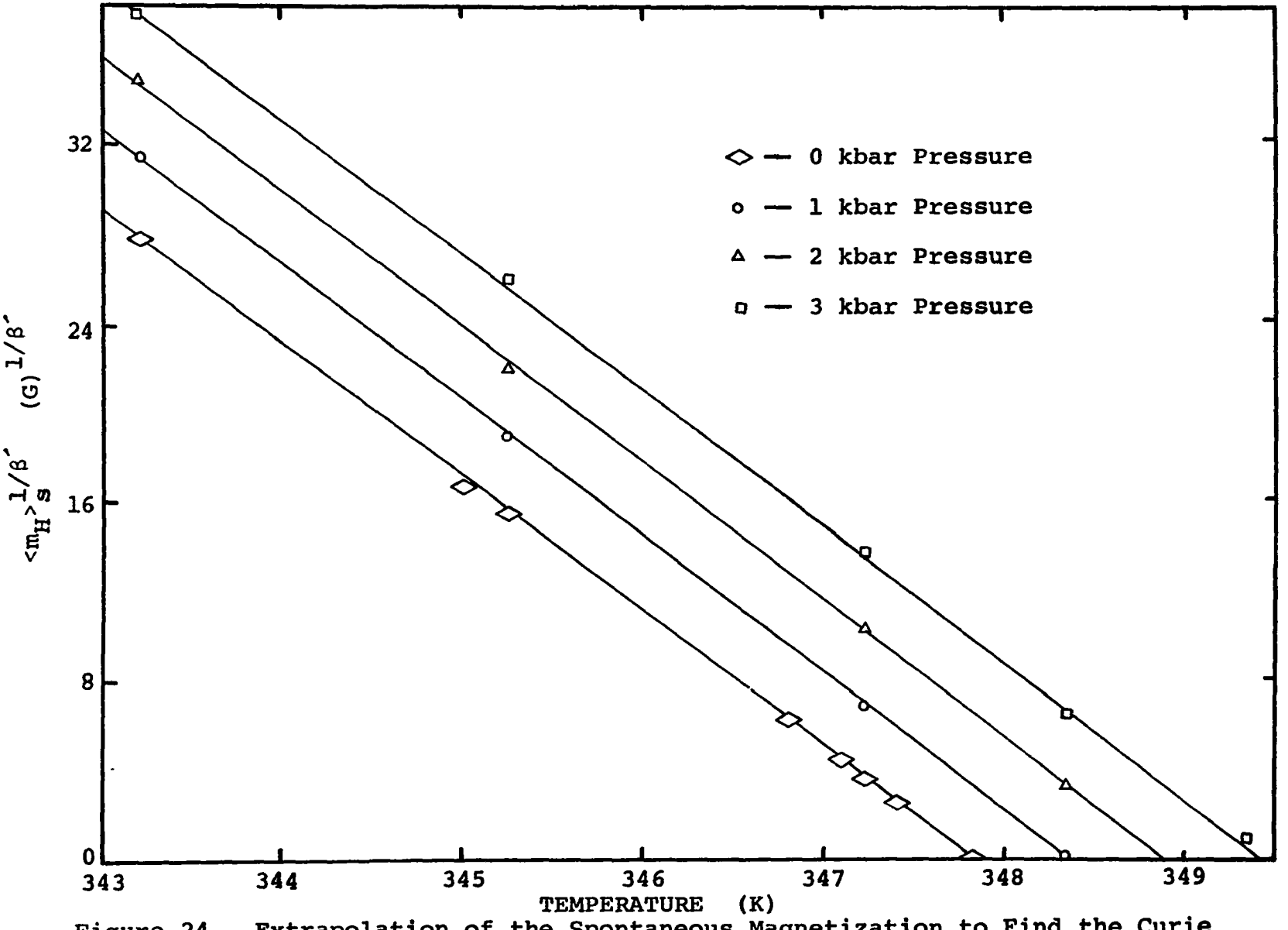

Figure 24. Extrapolation of the Spontaneous Magnetization to Find the Curie Temperature as a Function of Pressure.

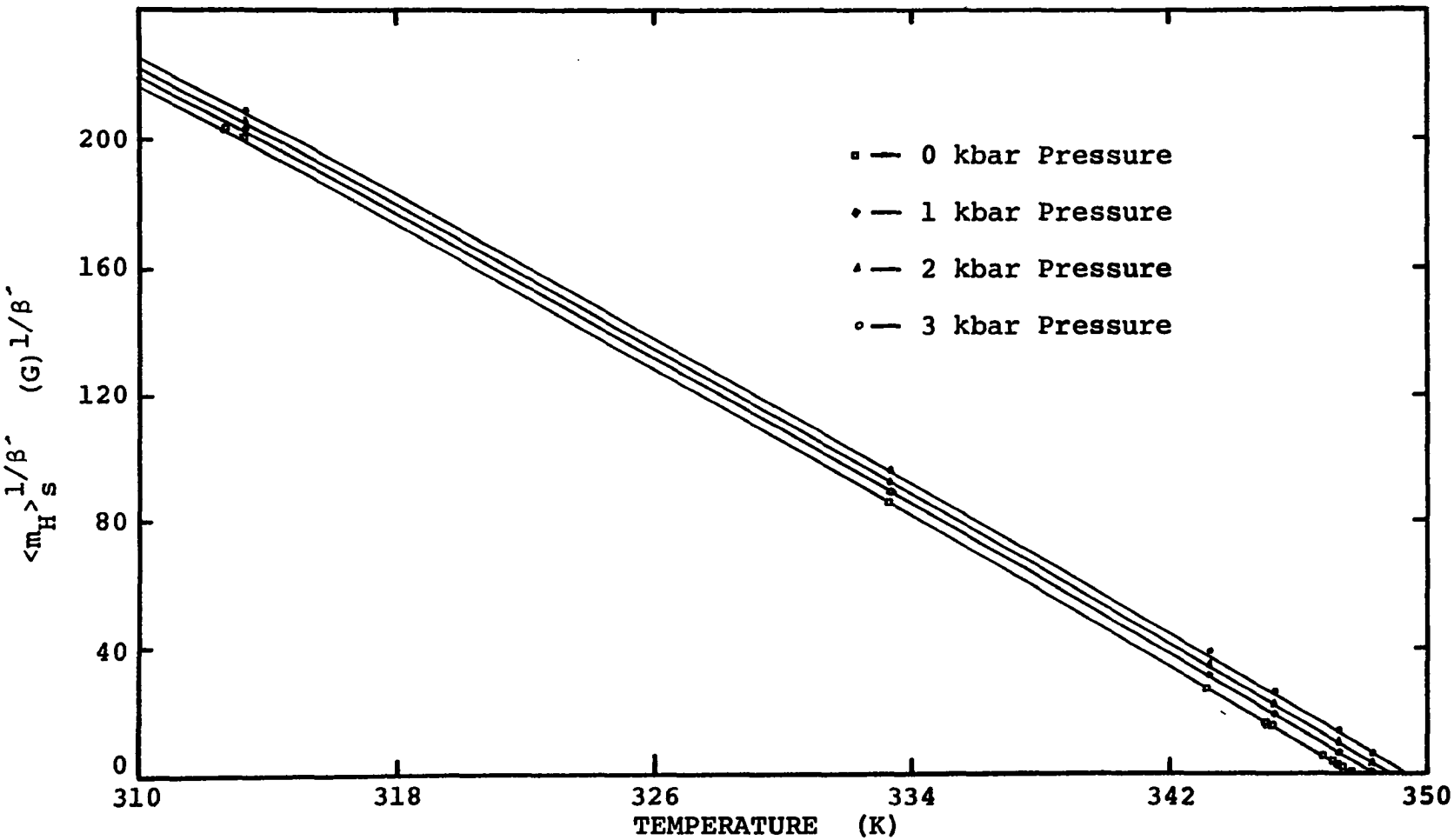

Figure 25. Spontaneous Magnetization as a Function of Temperature and Pressure.

down below this temperature.

Above T_c the initial susceptibility as a function of pressure is shown in Table VIII.

Table VIII. Initial Susceptibility as a Function of Pressure Above T_c

Temperature (K)	Initial Susceptibility (G/kOe)	Pressure (kbar)
349.34	0.41	1
351.16	0.2060	1
351.16	0.2235	2
351.16	0.2602	3
353.16	0.1785	1
353.16	0.1854	2
353.16	0.1926	3

Equation (21b) for the initial susceptibility can be inverted to give a function linearly proportional to temperature. Figure 26 shows a plot of this function versus temperature. There is insufficient data at 2 and 3 k bar pressure to estimate the corresponding T_c. Table IX gives the intercepts and their error.

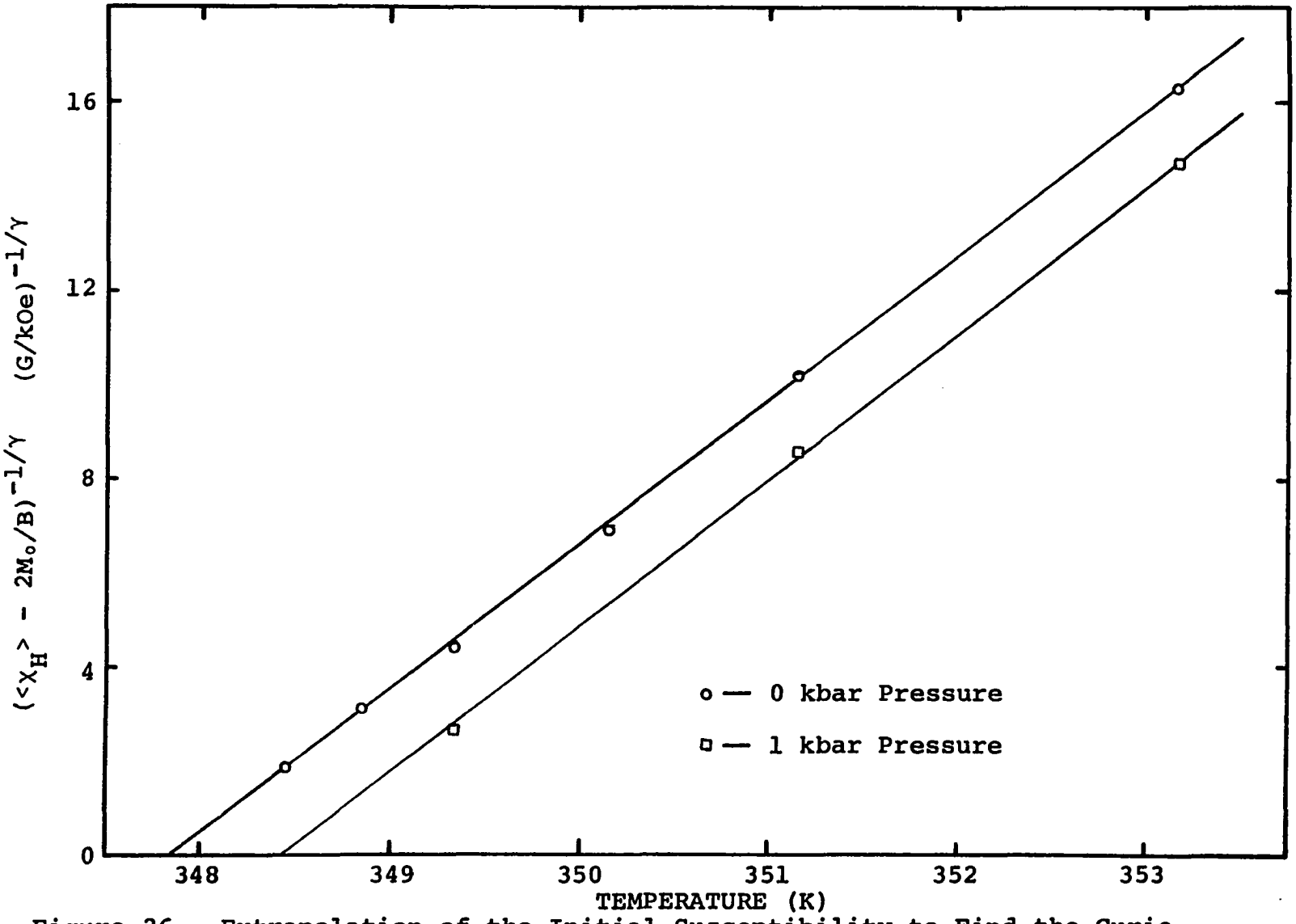

Figure 26. Extrapolation of the Initial Susceptibility to Find the Curie Temperature as a Function of Pressure.

Table IX. Curie Temperature as a Function of Pressure Determined from Initial Susceptibility

$T_c(p)$ (K)	Pressure (kbar)	$T_c(p) - T_c(0)$ (K)
347.85 ± 0.03	0	
348.45 ± 0.10	1 ± 0.02	0.60

The data below T_c is more accurate and will be averaged to find the change in Curie temperature with pressure. The result is

$$\Delta T_c/\Delta p = 0.52 \pm 0.03 \quad K/kbar$$

The error is twice the standard deviation of the mean. This $\Delta T_c/\Delta p$ adequately describes the effect of pressure on the magnetization.

CHAPTER VII

SUMMARY

This dissertation has investigated the magnetization of iron borate in the critical region. A vibrating coil magnetometer was used to measure the magnetization as a function of temperature, pressure, and magnetic field. The data was analyzed using a theory of weak ferromagnetism modified to agree more closely with scaling theory. Four critical exponents of $FeBO_3$ as well as the change in Curie temperature with pressure were obtained.

The initial step in the investigation was building and testing the magnetometer. The equipment was scaled to fit an available magnet. A vibrating coil magnetometer was desired because the environment of the sample could be more easily controlled. Two coils were used to reduce the sensitivity of the magnetometer to variation in sample placement. Fluid from a heat bath determined the temperature of the sample. Pressure was varied by a jack pump. The variation of the output voltage of the magnetometer caused by changes in the location of the sample agreed with that predicted by theory. The magnetometer was refined by making it into a null instrument. A pair of balance coils was added to cancel the dipole signal from the sample. The DC current in the balance coils which nulled the sample signal was proportional to the magnetization. This current could be precisely measured and was unaffected by

the non-linearities in the detection electronics.

The $FeBO_3$ sample was made by reacting Fe_2O_3 with B_2O_3. These components were mixed using an excess of B_2O_3 in a ball mill before heating in a vacuum at 800 C. The excess B_2O_3 was removed from the reacted product by washing with hot water. The iron borate was composed of 1 to 5 micron diameter green platelets. Both chemical and X-ray analyses showed that the sample was $FeBO_3$.

The sample was aligned in the magnetometer so that small changes in position had little effect on the magnitude of the signal. The magnetization was obtained from the difference between the sample-in and sample-out signals. Corrections were made for the sample holder and for the bulk compression when pressure was applied. The magnetometer was calibrated using the calculated magnetization of a current carrying coil. Because the sample was large enough to extend outside the region of maximum sensitivity of the pick-up coils, an adjustment to the calibration factor was necessary. Since the magnetization of $FeBO_3$ is low compared to that of iron or nickel, the correction for the demagnetizing field was small. Thus moderate errors in this correction did not effect the data.

The magnetization of iron borate was determined at selected values of the temperature, pressure, and magnetic field. A majority of the measurements were made at temperatures near T_C. The maximum pressure was limited to 3 kilobar and the magnetic field to 5 kilogauss.

Two modifications to the thermodynamic theory of weak ferromagnetism were developed. First, the temperature dependences of

the coefficients in the magnetic part of the free energy were chosen to make the magnetization agree more closely with scaling theory. Because of the approximations used, the equations for the magnetic susceptibilities near T_C were valid only in the limit of zero magnetic field. Second, the magnetization of a powdered sample had to be calculated for a partially aligned distribution of single crystals. Because the anisotropy field in the basal plane of $FeBO_3$ was small, the magnetization rotated in the basal plane of each crystal until it had a maximum component parallel to the applied magnetic field. This made the calculation of the magnetization for this powdered sample easy.

The data was analyzed using the modified theory. Near T_C an empirical adjustment was made for the effect of domains, etc. The Curie temperature, found from extrapolating the spontaneous magnetization to zero, was 347.85 ± 0.2 K. Above 320 K the spontaneous magnetization was proportional to $(T_C - T)^{\beta'}$. The value of β' was 0.350 ± 0.007 which agreed with published values.[8,9]

In order to obtain the initial differential susceptibility below T_C and the initial susceptibility above T_C the magnetization versus magnetic field was fit to an appropriate power series. The initial susceptibilities were determined from these power series. Below T_C the initial differential susceptibility increased as T_C was approached at a rate of $(T_C - T)^{-\gamma'}$ where γ' was 1.01 ± 0.10. Above T_C the susceptibility was proportional to $(T - T_C)^{-\gamma}$ where γ was 1.38 ± 0.08. That these two critical exponents are not equal is significant. Scaling theory has a simpler form when these

exponents are equal.

At T_c the magnetization and magnetic field are related by the critical exponent δ. We found that $\delta = 3.9 \pm 0.4$. This value differed from the value of 3 reported by Yakomov, Ozhogin, Gamlitskii, Cherepanov, and Pudkov;[9] their value was obtained by using another technique. Our data used to calculate δ was obtained when the temperature was within 0.03 K of T_c.

Hydrostatic pressure caused the Curie temperature to increase at a rate of 0.52 ± 0.03 K/kbar. The pressure induced shift in the magnetization could be matched by using an appropriate temperature change. Thus the critical exponents, to a first order, were unaffected by pressure.

APPENDIX I

CALCULATION OF FLUX IN THE PICK-UP COILS

The operation of the vibrating coil magnetometer is checked using the induction field of a current carrying coil and applying Faraday's law. In order to compare experimental results with theory a calculation is made of the flux in the pick-up coils as a function of position of the current carrying coil. The induced voltage is then calculated from the variations in the magnetic induction or in the position of the coils with time. A calculation of the flux is described below.

The coordinate system is shown in Figure 27. The origin is at the midpoint between the pick-up coils. Points on these pick-up coils are given by the unprimed coordinate system. The coil which is the source of the induction field is replaced by two magnetic surface poles. The primed coordinates refer to locations on these surface poles. The magnetic induction perpendicular to the face of a pick-up coil, B_z, is proportional to

$$B_z(x,y,z) \propto \iint [(z-L)/r_1^3 + (z+L)/r_2^3]\, dx'\, dy'$$

where

L = 0.635 cm, half the distance between the magnetic surface poles,

$r_1^2 = (x-x')^2 + (y-y')^2 + (z-L)^2$, and

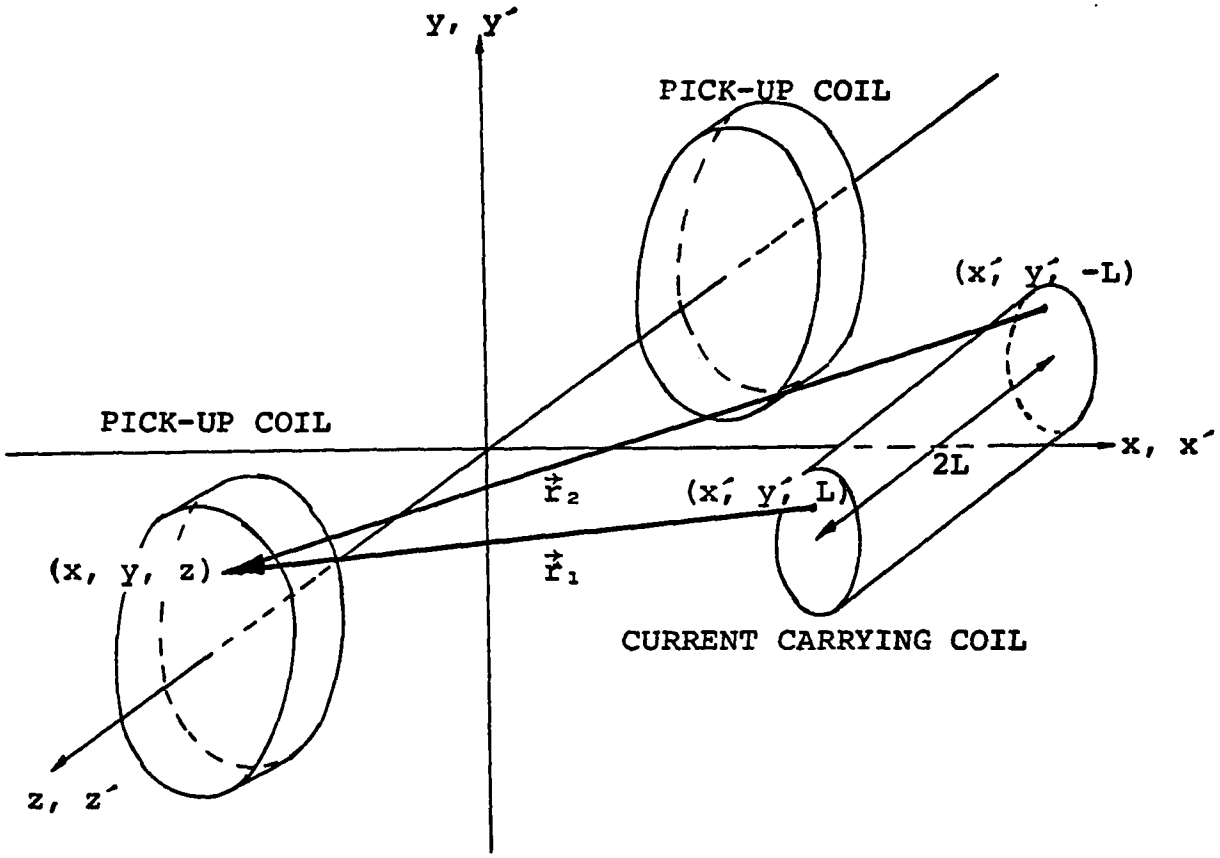

Figure 27. Coordinate System for Calculating the Flux in the Pick-up Coils. The origin for both the primed and unprimed coordinates is on the axis midway between the pick-up coils. The primed coordinates refer to locations on the end surfaces of the current carrying coil. The flux is calculated at various (x, y, z) positions in the pick-up coils.

$$r_2^2 = (x-x')^2 + (y-y')^2 + (z+L)^2.$$

The integral extends over the area of a surface pole which has a radius of 0.319 cm. The y′ integration is done analytically; the subsequent x′ integration is performed on a computer. The integral is evaluated at 1806 points covering a xyz-grid of 43 x 14 x 3 values respectively. The three values of z correspond to the position of the front, middle, and back layers of a pick-up coil. When all the coils are coaxial, the x′ integration can also be done analytically. The computer calculation of B_z checks with the analytically determined value for this configuration.

The flux through each of the three layers of the pick-up coil is obtained by summing the weighted flux associated with each grid point in a layer. The weighting factor is the number of turns in a layer enclosing each grid point. The total flux is the sum from the three layers with the middle layer weighted by a factor of four (Simpson's rule). The total flux as a function of the position of the current carrying coil is shown in Figure 2, Chapter II. The flux is scaled to agree with experiment when the pick-up coils and the current carrying coil are coaxial.

APPENDIX II

DETAILED SAMPLE PREPARATION AND ANALYSIS

Iron borate is made by combining Fe_2O_3 and B_2O_3 in equal molar ratios. An outline of the procedure to accomplish this is as follows:

1. Boric oxide, pulverized in a ball mill, and finely powdered ferric oxide are intimately mixed. This is done by ball milling the combined components for 4 hours. The 5.6:1 molar ratio of B_2O_3 to Fe_2O_3 used drives the reaction product away from Fe_3BO_6.
2. The sample is placed in a quartz tube and heated to 190°C. This heated tube is then evacuated for 45 minutes to remove absorbed and hydrated water. After the evacuated tube is sealed there will be no water vapor released to build up pressure in the tube.
3. The firing schedule is 36 hours at 600°C followed by 120 hours at 800°C. The reaction product is brought to room temperature in two steps. The sample is cooled at a rate of 25°C/hour for 12 hours. After 18 hours at 500°C the furnace is turned off and the sample is cooled to room temperature at the rate governed by the closed furnace. The quartz tube cracks into many chips before room temperature is

reached.

4. Excess B_2O_3 is removed by washing with hot distilled water six to ten times. The $FeBO_3$ is separated from the fine quartz chips using a magnet. This remaining material is a finely divided, green powder.

The chemicals used were Reagent Grade A.C.S. boric oxide, Matheson, Coleman, and Bell and ferric oxide (99.9%) Alfa Inorganics Division, Ventron.

The amount of iron in the reaction product is determined by dissolving a small sample in acid, reducing the iron to Fe^{+2} and titrating to Fe^{+3} with potassium dichromate. The general method, given in Standard Methods of Chemical Analysis,[31] is followed except that perchloric acid is used instead of hydrochloric. The boron content is obtained by first removing the iron and then titrating the boric acid with sodium hydroxide as described in the same book.[31] Known mixtures of ferric oxide and boron oxide, in the proper ratio, are analyzed to verify the chemical procedures.

The results of the titrations are given in Chapter III. The errors are estimated from the accuracy of analyzing the known samples. Within the error of the analysis, material made by the method outlined above has the proper iron/boron ratio for $FeBO_3$.

APPENDIX III

TABLES OF MAGNETIZATION FOR $FeBO_3$

The magnetization of $FeBO_3$ in gauss as a function of temperature, pressure and magnetic field is given below. The magnetic field is corrected for the demagnetizing field of the sample. Atmospheric pressure is recorded as 0 kbar. Corrections to the magnetization are made for the sample holder and sample compression when pressure is applied. The calibration of the magnetometer is adjusted for the 'size' of the sample.

T = 20.11°C

p = 0 kbar

H (Oe)	M (G)
564	7.286
963	7.493
1462	7.645
1962	7.760
2961	7.943
3960	8.113
4959	8.278

T = 39.55°C

p = 0 kbar

H (Oe)	M (G)
569	6.364
968	6.528
1467	6.652
1967	6.749
2966	6.918
3965	7.084
4964	7.247

T = 40.09°C

p = 0 kbar		p = 1 kbar		p = 2 kbar		p = 3 kbar	
H (Oe)	M (G)	H (Oe)	M (G)	H (Oe)	M (G)	H (Oe)	M (G)
569	6.316	569	6.335	569	6.370	569	6.407
968	6.465	968	6.648	968	6.677	968	6.715
1467	6.641						
1967	6.709						
2966	6.885						
3965	7.047						
4965	7.217						

T = 60.00°C

p = 0 kbar		p = 1 kbar		p = 2 kbar		p = 3 kbar	
H (Oe)	M (G)	H (Oe)	M (G)	H (Oe)	M (G)	H (Oe)	M (G)
377	4.683						
577	4.778	576	4.840	576	4.896	576	4.951
		576	4.832	576	4.888		
976	4.882	976	4.927	975	5.003	975	5.064
		976	4.949	975	5.007		
1476	4.995	1476	5.037	1476	5.123	1475	5.176
		1476	5.053	1476	5.106	1475	5.179
		1476	5.054	1476	5.121		
1975	5.078	1975	5.136	1974	5.205	1974	5.276
		1975	5.149	1974	5.213		
2974	5.241	2974	5.308	2974	5.375	2973	5.438
		2974	5.306	2974	5.371		
3973	5.408	3973	5.473	3973	5.541	3973	5.631
		3973	5.491	3973	5.557		
4973	5.570	4972	5.621	4972	5.700	4972	5.780
		4972	5.633	4972	5.698		

T = 70.02°C

p = 0 kbar

H (Oe)	M (G)
384	3.201
584	3.254
984	3.340
1483	3.439
1983	3.530
2982	3.703
3981	3.869
4980	4.019

T = 70.06°C

p = 0 kbar		p = 1 kbar		p = 2 kbar		p = 3 kbar	
H (Oe)	M (G)	H (Oe)	M (G)	H (Oe)	M (G)	H (Oe)	M (G)
185	3.085						
384	3.194						
584	3.242	583	3.371	583	3.493	582	3.610
984	3.342						
1483	3.432	1482	3.566	1482	3.688	1481	3.801
1983	3.523						
2982	3.695	2981	3.827	2981	3.960	2980	4.064
3981	3.862						
4980	4.014	4980	4.139	4979	4.269	4978	4.384

T = 71.88°C

p = 0 kbar

H (Oe)	M (G)
187	2.619
387	2.704
587	2.745
986	2.830
1486	2.927
1985	3.011
2984	3.192
3984	3.365
4983	3.530

T = 72.10°C

p = 0 kbar		p = 1 kbar		p = 2 kbar		p = 3 kbar	
H (Oe)	M (G)	H (Oe)	M (G)	H (Oe)	M (G)	H (Oe)	M (G)
188	2.548						
387	2.629						
587	2.671	586	2.859	585	3.023	584	3.182
986	2.764						
1486	2.863	1485	3.050	1484	3.205	1483	3.392
1986	2.947	1985	3.135	1984	3.300	1983	3.447
2985	3.117						
3984	3.287	3983	3.463	3982	3.626	3981	3.767
4983	3.454						

T = 73.65°C

p = 0 kbar

H (Oe)	M (G)
391	1.938
590	1.998
990	2.081
1489	2.192
1989	2.293
2988	2.490
3987	2.681
4986	2.875

T = 73.94°C

p = 0 kbar

H (Oe)	M (G)
192	1.648
392	1.731
591	1.792
991	1.888
1490	1.996
1990	2.102
2989	2.313
3988	2.518
4987	2.717

T = 74.07°C

p = 0 kbar		p = 1 kbar		p = 2 kbar		p = 3 kbar	
H (Oe)	M (G)	H (Oe)	M (G)	H (Oe)	M (G)	H (Oe)	M (G)
147	1.535						
192	1.570						
392	1.631	390	1.995	389	2.278	388	2.507
592	1.693						
991	1.798	989	2.154	988	2.434	987	2.664
1491	1.915						
1990	2.028	1988	2.365	1987	2.627	1986	2.855
2490	2.133						
2989	2.232	2987	2.565	2986	2.804	2985	3.025
3988	2.460						
4987	2.638	4986	2.909	4985	3.140	4984	3.349

T = 74.25°C

p = 0 kbar

H (Oe)	M (G)
593	1.535
992	1.653
1491	1.783
1991	1.903
2990	2.126
3989	2.339
4988	2.541

T = 74.67°C

p = 0 kbar

H (Oe)	M (G)
38	0.446
97	0.555
147	0.613
197	0.668
396	0.821
595	0.946
995	1.125
1494	1.311
1993	1.470
2991	1.744
3990	1.989
4989	2.220

T = 74.93°C

p = 0 kbar

H (Oe)	M (G)
39	0.141
99	0.224
198	0.335
398	0.517
597	0.660
996	0.878
1495	1.088
1994	1.265
2992	1.577
3991	1.831
4990	2.054

T = 75.18°C

p = 0 kbar		p = 1 kbar		p = 2 kbar		p = 3 kbar	
H (Oe)	M (G)	H (Oe)	M (G)	H (Oe)	M (G)	H (Oe)	M (G)
199	0.149	197	0.699	193	1.485	191	1.874
299	0.206						
399	0.269	396	0.849	392	1.558	390	1.951
598	0.381						
997	0.594	994	1.194	991	1.747	990	2.116
1496	0.817						
1995	0.997	1993	1.502	1990	1.988	1989	2.332
2994	1.315						
3992	1.585	3990	2.036	3988	2.392	3987	2.688
4991	1.841						

T = 75.30°C

p = 0 kbar

H (Oe)	M (G)
40	0.0407
100	0.0760
150	0.0967
199	0.125
399	0.222
599	0.314
998	0.488
1497	0.689
1996	0.874
2994	1.195
3993	1.486
4991	1.754

T = 75.70°C

p = 0 kbar

H (Oe)	M (G)
100	0.0528
150	0.0659
200	0.0846
399	0.155
599	0.226
998	0.365
1497	0.535
1997	0.696
2995	0.994
3994	1.272
4992	1.544

T = 76.18°C

p = 0 kbar		p = 1 kbar		p = 2 kbar		p = 3 kbar	
H (Oe)	M (G)	H (Oe)	M (G)	H (Oe)	M (G)	H (Oe)	M (G)
100	0.0295	100	0.0492	99	0.153		
150	0.0417						
200	0.0611	200	0.0946	199	0.249		
300	0.0944						
399	0.124	399	0.177	398	0.417	394	1.181
599	0.175						
999	0.284	998	0.397	996	0.745	993	1.401
1498	0.422						
1997	0.559	1996	0.748	1994	1.166	1992	1.699
2996	0.821						
3995	1.073	3993	1.357	3991	1.754	3989	2.174
4994	1.310						

T = 77.00°C

p = 0 kbar

H (Oe)	M (G)
999	0.224
1998	0.446
2997	0.665
3996	0.880
4995	1.094

T = 78.00°C

p = 0 kbar		p = 1 kbar		p = 2 kbar		p = 3 kbar	
H (Oe)	M (G)	H (Oe)	M (G)	H (Oe)	M (G)	H (Oe)	M (G)
40	0.0104						
100	0.0220						
150	0.0256						
200	0.0369						
400	0.0757						
599	0.115	599	0.123	599	0.136	599	0.161
999	0.192						
1499	0.282	1498	0.309	1498	0.342	1498	0.399
1998	0.389						
2997	0.583	2997	0.618	2997	0.668	2996	0.778
3996	0.778						
4995	0.974						

T = 80.00°C

p = 0 kbar		p = 1 kbar		p = 2 kbar		p = 3 kbar	
H (Oe)	M (G)	H (Oe)	M (G)	H (Oe)	M (G)	H (Oe)	M (G)
999	0.174	999	0.177	999	0.184	999	0.192
1998	0.351	1998	0.358	1998	0.372	1998	0.389
2997	0.523	2996	0.536	2996	0.555	2996	0.576
3997	0.704						
4996	0.874						

T = 82.00°C

p = 0 kbar

H (Oe)	M (G)
999	0.167
1998	0.329
2998	0.494
3997	0.562
4996	0.833

T = 90.00°C

p = 0 kbar

H (Oe)	M (G)
999	0.157
1998	0.317
2998	0.475
3997	0.631
4996	0.792

p = 3 kbar

H (Oe)	M (G)
999	0.160
1998	0.325
2998	0.483

T = 100.00°C

p = 0 kbar

H (Oe)	M (G)
999	0.156
1999	0.307
2998	0.464
3997	0.622
4996	0.776

REFERENCES

1. I. Bernal, C. W. Struck, and J. G. White, Acta Cryst. 16, 849 (1963).
2. A. J. Kurtzig, R. Wolfe, R. C. LeCraw and J. W. Nielsen, Appl. Phys. Lett. 14, 350 (1969).
3. J. F. Dillon, J. Appl. Phys. 39, 922 (1968).
4. R. Wolfe, A. J. Kurtzig, and R. C. LeCraw, J. Appl. Phys. 41, 1218 (1970).
5. Michel Pernet, David Elmaleh, and Jean-Claude Joubert, Solid State Comm. 8, 1583 (1970).
6. V. D. Doroshev, N. M. Kovtun, V. N. Seleznev and V. M. Siryuk, ZhETF Pisma Red. 13, 672 (1971), JETP Lett. 13, 475 (1971).
7. M. P. Petrov, G. A. Smolensky, A. P. Paugurt and S. A. Kighaev, AIP Conf. Proc. 5, 379 (1971).
8. M. Eibschutz, L. Pfeiffer, and J. W. Nielsen, J. Appl. Phys. 41, 1276 (1970).
9. S. S. Yakimov, V. I. Ozhogin, V. Ya. Gamlitskii, V. M. Cherepanov, and S. D. Pudkov, Phys. Letters 39A, 421 (1972).
10. D. O. Smith, Rev. Sci. Instrum. 27, 261 (1956).
11. K. Dwight, N. Menyuk, and D. Smith, J. Appl. Phys. 29, 491 (1958).
12. J. C. Joubert, T. Shirk, W. B. White, and Rustum Roy, Mater. Res. Bull. 3, 671 (1968).
13. I. E. Dzialoshinsky, JETP 32, 1547 (1957), Soviet Phys. JETP 5, 1259 (1957).

14. A. S. Borovik-Romanov and V. I. Ozhogin, JETP 39, 27 (1960), Soviet Phys. JETP 12, 18 (1961).

15. R. E. Stoner, R. H. Herbert, and L. R. Sill, Appl. Phys. 41, 3706 (1970).

16. T. R. McGuire and P. J. Flanders, Magnetism and Metallurgy, ed. Berkowitz and Kneller, (Academic Press, New York, 1969), p. 165.

17. National Bureau of Standards Circular 561, (1955).

18. Helmy Markam, Louis Touron, and Jean Lories, J. Crys. Growth 13/14, 585 (1972).

19. R. C. LeCraw, R. Wolfe, and J. W. Nielsen, Appl. Phys. Lett. 14, 352 (1969).

20. T. A. Grigor'eva and A. V. Nikolaev, Dokl. Akad. Nauk SSSR 181, 1381 (1968), Dokl. Chemistry 181, 753 (1968).

21. E. C. Stoner, Phil. Mag. 36, 803 (1945).

22. Toru Moriya, Phys. Rev. 120, 91 (1960).

23. Toru Moriya, in Magnetism, ed. G. T. Rado and H. Suhl, (Academic Press, New York, 1964) Vol. I, p. 112.

24. L. D. Landau and E. M. Lifshitz, Statistical Physics (Addison-Wesley, Reading, Mass., 1958), pp. 430-9.

25. K. P. Belov, Magnetic Transitions, trans. W. H. Furry, (Consultants Bureau Enterprises, New York, 1961).

26. Landau and Lifshitz, p. 436.

27. Robert Brout, in Statistical Mechanics, ed. S. A. Rice et al, (University of Chicago Press, 1972), pp. 279-98.

28. Louis Brand, Advanced Calculus, John Wiley, New York, 1958).

29. L. Patrick, Phys. Rev. 93, 384 (1954).

30. E. G. Rudashevsky, V. N. Seleznyov and L. V. Velikov, Solid State Comm. 11, 959 (1972).

31. N. Howell Furman, ed., Standard Methods of Chemical Analysis 6th ed., Vol. 1 (D. van Nostrand, Princeton, N. J., 1962) pp. 218-23, 538-44.